Universität Potsdam
Mathematisch-naturwissenschaftliche Fakultät
Institut für Erd- und Umweltwissenschaften
Studiengang: Geoökologie

Master thesis

Organic Matter Characteristics in a Changing Permafrost Environment: Yukechi Alas Landscape, Central Yakutia

vorgelegt von: Torben Windirsch
Matrikel-Nr.: 770855
E-Mail: torben.windirsch@uni-potsdam.de

Gutachter: Dr. Jens Strauss
Zweitgutachter: Prof. Dr. Guido Grosse

Abgabetermin: August 2018
Bearbeitungszeit: 6 Monate

Table of contents

Table of figures

List of tables

Abstract

With alarmingly fast climate change on global scale, the origin of carbon emissions is becoming more important. Permafrost as one of the largest terrestrial natural storages is among the most relevant carbon sinks that might become a carbon source as air temperatures and snowfall are increasing. This study examines the Yukechi Alas area (N 61.76495° / E 130.46664°), a landscape in Central Yakutia, located on the Abalakh terrace in the Lena-Aldan interfluve). Two drilling cores from different ground types were taken. The comparison of the both cores used in this study also gives insights into the development of permafrost carbon storage. One is a Yedoma core, consisting of material accumulated and syngenetically frozen during the late Pleistocene. The second core was taken from an adjacent alas basin. Alas deposits in this area are altered Yedoma deposits thawed and subsided after lake formation. Both cores cover a timespan of approximately 50 000 years. The cores were analysed for ice content, total carbon and total nitrogen content, total organic carbon content, stable oxygen and hydrogen isotopes, stable carbon isotopes, mass specific magnetic susceptibility and grain size distribution, and were dated using radiocarbon measurements. The laboratory analyses revealed some interesting features that are quite uncommon for Yedoma deposits globally but have been found in Central Yakutia before. The most astonishing finding is the lack of carbon over several meters depth, found in both cores. While in the alas core this could hint on deep thawing during lake-covered stages and large talik formation, and hence decomposition, the same finding in the Yedoma core indicate sediment input of organic-poor material. Water isotope data derived from pore ice show a permanently frozen state of the lower core parts and only represent precipitation water very close to the surface. Therefore, it is unlikely that strong organic matter decomposition took place in this Yedoma core. Also, these core parts consist of more coarse material. Fine sand is found here instead of the silty material that makes up most of the cores. This change in material input was dated to a timespan between 39 000 and 18 000 years before present. During this time, climate experienced variations on a global as well as on a regional scale, which could have influenced the availability of liquid water as well as thaw depth and wind regimes. Especially the changes in wind direction and velocity are likely to have influenced the material composition. The sandy material found is not originating from surrounding areas but could be transported over greater distances. These findings indicate that Yedoma might be more heterogeneous on a global scale than previously thought, making it important to further study Yedoma deposits. Both general carbon content as well as carbon vulnerability, for example due to alternating sediment characteristics within a Yedoma deposit, might be very different. It can be assumed that, before thermokarst processes occured, the core drilled within the alas basin had quite similar characteristics as the Yedoma core. This indicates possible developing characteristics of Yedoma deposits during ongoing climate change. A possible reason for this is increasing lake formation in Arctic areas due to warming air temperatures, which in turn can lead to further carbon release with further permafrost thaw, enhancing a positive feedback cycle in Northern permafrost areas.

German summary / deutsche Kurzfassung

Im Zuge des globalen Klimawandels wird die Einschätzung möglicher Kohlenstoffquellen zunehmend wichtiger. Permafrostböden als einer der größten terrestrischen Kohlenstoffspeicher ist dabei von besonderem Interesse, da in einem wärmeren Klima diese Böden auftauen könnten und große Mengen Kohlenstoff freisetzen könnten, die zu einer weiteren Klimaerwärmung beitrügen. Diese Arbeit beschäftigt sich mit Permafrost im Gebiet des Yukechi Alas in Zentraljakutien. Das Untersuchungsgebiet liegt auf der Abalakh-Terrasse der Lena, im Gebiet zwischen den Flüssen Lena und Aldan. Für die Untersuchung wurden zwei Bohrkerne aus unterschiedlichen Typen von Permafrostböden entnommen. Diese Kerne wurden anschließend unterbeprobt und auf die Parameter Eisgehalt, Gesamtkohlenstoff-, Gesamtstickstoff- und organischer Gesamtkohlenstoffgehalt, Sauerstoff-, Wasserstoff- und Kohlenstoffisotopenverhältnisse, massenspezifische magnetische Suszeptibilität, Korngrößenverteilung und Radiokarbonalter hin untersucht. Der erste Kern stammt aus einer Yedoma-Ablagerung, welche überwiegend aus spätpleistozänen Sedimenten besteht, welche während ihrer Ablagerung einfroren und seither gefroren sind. Der zweite Kern stammt aus einem benachbarten Alas-Bassin, das sich im regionalen Yedoma entwickelt hat, so dass davon auszugehen ist, dass das Material dieses Kerns vor der Überprägung durch einen Thermokarstsee sehr ähnlich zu dem Material des ersten Kerns war. Datierungen zeigen, dass beide Kerne eine Zeitspanne von rund 50 000 Jahren vor 1950 abdecken. Die Laboranalysen zeigen für Yedoma-Ablagerungen untypische Charakteristika, die aber in dieser Region bereits an anderer Stelle ebenfalls in ähnlicher Form gefunden wurden. Das auffälligste Merkmal ist eine mehrere Meter mächtige Schicht, die keine nachweisbaren Mengen Kohlenstoffs enthält und in beiden Kernen in unterschiedlicher Tiefe zu finden ist. Während sich dies im Alas-Kern durch tiefes Tauen des Bodens und demnach Kohlenstoffabbauprozesse während der Existenz eines Sees an der Landoberfläche zu erklären ist, deuten diese Funde im Yedoma-Kern auf eine veränderte und besonders sehr kohlenstoffarme Zusammensetzung des in diesem Zeitraum abgelagerten Materials hin. Dieses Material ist gröber als das der restlichen Kernabschnitte, was auf eine andere Herkunft des Materials schließen lässt. Die Tatsache, dass Wasserisotopendaten aus dem im Boden enthaltenen Eis zeigen, dass es sich um altes Eis und nicht später eingedrungenes und gefrorenes Regenwasser handelt, schließt einen derartig starken Abbau des Kohlenstoffes nach der Ablagerung des Yedoma-Materials aus. Eine mögliche Erklärung für Materialeintrag aus anderen Gebieten liefern die Ergebnisse der Datierung. Sie weisen für die gröberen, kohlenstoffarmen Schichten in beiden Kernen einen Ablagerungszeitraum von 39 000 bis 18 000 Jahren vor 1950 aus. Zu beiden Zeitpunkten gab es Variationen sowohl im globalen als auch im regionalen Klima Zentraljakutiens, die die Verfügbarkeit flüssigen Wassers sowie die sommerlichen Autautiefe des Bodens und Hauptwindrichtung und -geschwindigkeit beeinflussten. Da das in diesen Schichten gefundene Material aus anderen Gebieten transportiert worden sein muss, kommt besonders die Veränderung des Windregimes als Grund für die andersartige Materialzusammensetzung in Frage. Diese Ergebnisse zeigen, dass die als Kohlenstoffspeicher von globaler Bedeutung verstandenen Yedoma-Ablagerungen auf globaler Skala deutlich heterogener sein könnten als bisher angenommen. Dies würde sich auch auf die bislang angenommenen Anfälligkeiten gegenüber Tauprozessen und damit Kohlenstofffreisetzung auswirken, da unterschiedliche abgelagerte Materialien diesbezüglich unterschiedliche Eigenschaften aufweisen. Diese Vergleichsstudie zeigt außerdem, ausgehend von der Hypothese, die Alas-Ablagerungen seien, vor der Entstehung eines Thermokarst-Sees an der Landoberfläche, den Yedoma-Ablagerungen sehr ähnlich gewesen, wie sich die momentan noch existierenden Yedoma-Ablagerungen in einem voranschreitenden Klimawandel verhalten könnten. Die Tatsache, dass immer noch, trotz zwischenzeitlichen Tauens, Kohlenstoff in den Alas-Ablagerungen enthalten ist, ermöglicht eventuell genauere Abschätzungen über die zu erwartenden Kohlenstoffemissionen aus Permafrostböden im Zuge des Klimawandels.

1 Introduction

1.1 Permafrost

Permafrost regions store big amounts of carbon, which makes them vulnerable regions for climate warming. The currently stored carbon could be released to the atmosphere upon permafrost thaw and function as a positive feedback to climate warming. Especially during the late Pleistocene and the Holocene, permafrost areas represented an important carbon sink for global climate, but could now become a carbon source. To understand the implications of permafrost thaw on the global climate, deeper insight into processes related to permafrost carbon transport is needed.

Permafrost is a term used for any type of ground, either soil or rock, that maintains temperatures below 0 °C for more than two consecutive years (van Everdingen, 2005; Heginbottom et al., 2012). It occurs in non-glaciated Arctic and Antarctic regions, as well as in alpine regions that provide mean annual temperatures below 0 °C (**Figure 1**) (Brown et al., 2002, 1997). Permafrost covers approx. 22 % of the Northern Hemisphere's terrestrial surface (Zhang et al., 1999). There are various permafrost zones differentiated by continuity, including the continuous permafrost zone (> 90 % of the area are permafrost), discontinuous permafrost zone (50-90 %), sporadic permafrost zone (10-50 %) and isolated permafrost zone (< 10 %) (**Figure 1**) (Brown et al., 2002). Besides coverage, permafrost is also classified by its ice type and ice content. Permafrost containing more than 25 vol% ice is called ice-rich permafrost, while less than 25 vol% is called ice-poor (Brown et al., 2002). High ice content can be e. g. massive ground ice, which can either be a buried ice block originating from a glacier or an ice wedge that was formed by liquid water seeping into the ground and freezing there, or excess ice, when all pores in the ground were water filled and froze, forming larger, connected ice clusters. Permafrost terrain is typically characterized by three subsurface units: 1) The active layer lies on top of the permafrost table and seasonally thaws every summer. This allows for plant growth and decomposition during unfrozen summer conditions (van Everdingen, 2005); 2) Underneath lies the permafrost, which stays below 0 °C all year; 3) The permafrost depth is determined by the magnitude and duration of negative mean annual ground temperatures, as well as the geothermal heat flux. Therefore, unfrozen ground underlies permafrost. The permafrost contains the depth of zero annual amplitude (ZAA) in where a steady temperature is maintained all year (French, 2007). Permafrost can reach as deep as approx. 1450 m below surface (BS) in Eastern Siberia (Schuur et al., 2008). Due to local temperature differences, induced e. g. by ponding water, unfrozen areas called taliks may occur within the permafrost zone (Ferrians et al., 1969). Some special types of permafrost are e.g. Yedoma Ice Complex, which are an ice-rich (50-90 vol% ice) and organic bearing (ca. 2 wt%) (Schirrmeister et al., 2013) deposit originating from the late Pleistocene era (60 000 to 11 700 years before present (BP)). Alas is a local name, originating from Yakutia, for a drained and often refrozen former lake basin (including refrozen taliks). Deposits with thawing phases, like alas deposits, are assumed to show more characteristics of organic matter decomposition compared to permafrost that has been frozen since deposition (Strauss et al., 2015; Weiss et al., 2016; Jongejans et al., 2018). The processes in permafrost regions leading to the formation of those basins is thermokarst processes. Thermokarst is induced by thawing of permafrost or ground ice melt, often as a result of surficial water ponding, and subsequent surface subsidence (van Everdingen, 2005).

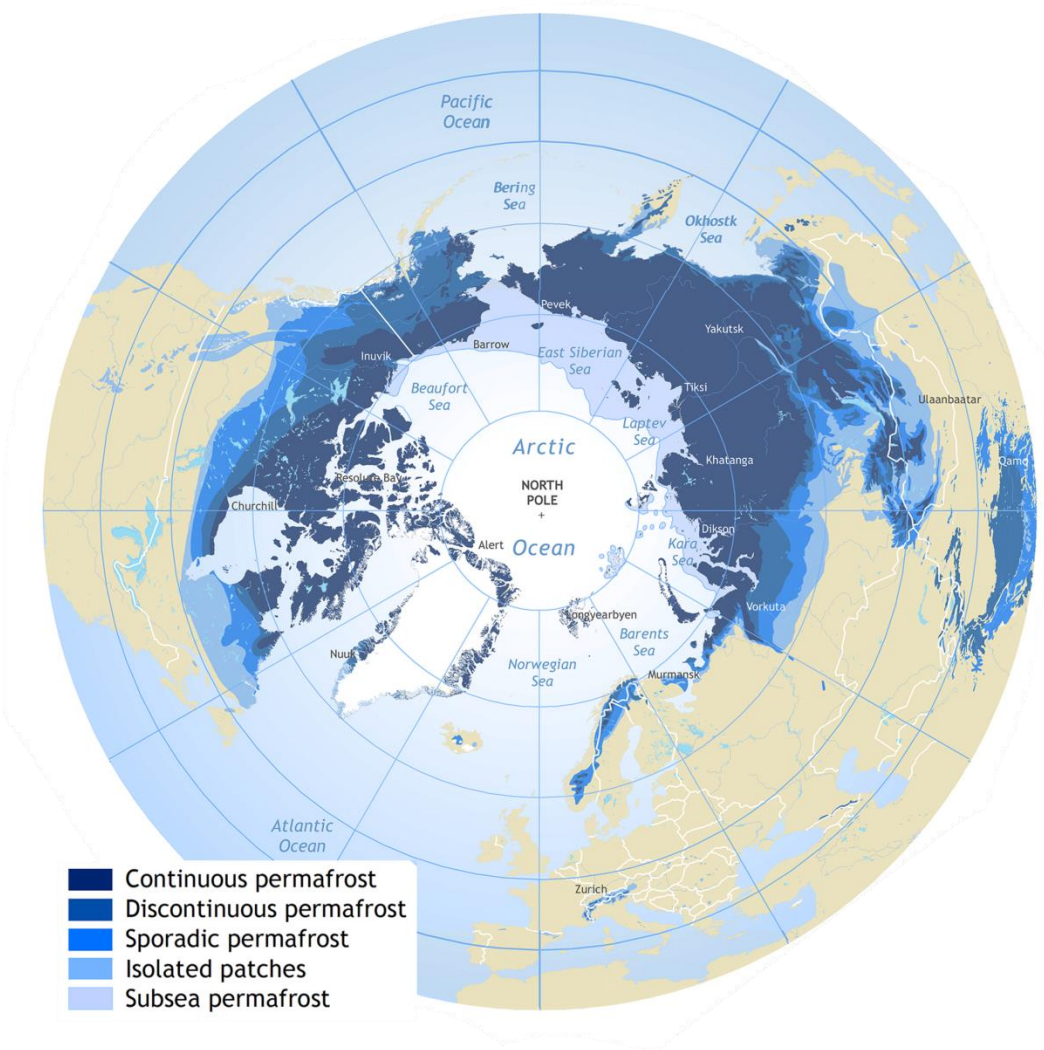

Figure 1 – Northern permafrost distribution (Brown et al., 1997); circumpolar map displaying the distribution of the different permafrost zones on the Northern Hemisphere

1.2 Carbon accumulation

As terrestrial permafrost is defined by temperatures at or below 0 °C for at least 2 consecutive years, organic matter decomposition is strongly reduced. Organic matter accumulates in the active layer and is subsequently incorporated into permafrost through ongoing accumulation or relative permafrost table aggradation. Moreover, cooling temperature raise decreases active layer thickness, causing the permafrost table to aggrade. Carbon accumulation is linked to plant growth, both in situ growth and off-site growth with lateral transport into the study area. However, lateral transport is very limited in most permafrost areas, as only three to four months provide warm enough air temperatures for the active layer to thaw, liquid water, and finally temperatures above 4 °C which is inevitable for plant growth (Hunt, 1982). Carbon in permafrost soils accumulates during phases with no ice cover. As this accumulation took place over long time periods, the current carbon content stored in circumpolar permafrost regions is estimated to be more than 1300 petagrams (Pg; 1 Pg = 1 billion tons), of which 800 Pg are set in permafrost (Hugelius et al., 2014; Strauss et al., 2015).

1.3 Research aims

The aim of this study is to understand the past and current state of Central Yakutian permafrost areas and their development processes in terms of organic carbon accumulation and storage. The major research questions are:

- How are Yedoma ice complex and the thermokarst basins biogeochemically and sedimentologically connected
- What are the main regional processes in carbon storage and history, and
- What is the potential future pathway of this permafrost conditions and their importance for global climate change

2 Study area

Two drilling cores were used for this study. They were obtained in the continuous permafrost zone in the Lena-Aldan interfluve (**Figure 2a**) in the Yukechi Alas (N 61.76495° / E 130.46664°), 80 km southeast of Yakutsk (Fedorov and Konstantinov, 2003), located in Central Yakutia, Russia. The Yukechi Alas is approx. 500 m in diameter and 10 to 15 m deep (**Figures 2b** and **3**).

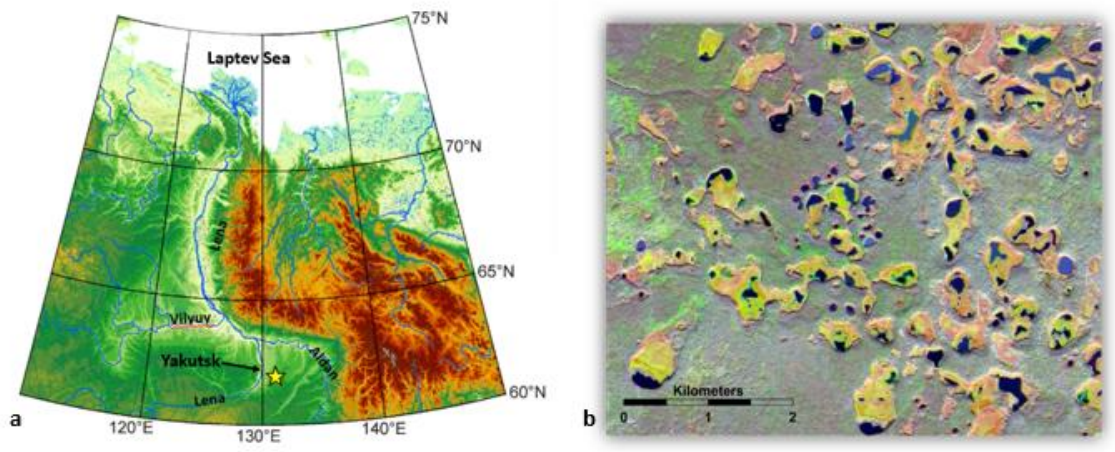

Figure 2 - a: location of Yakutsk (DEM: ESA DUE Permafrost project (Bartsch and Seifert, 2012)); b: satellite image of the Yukechi Alas, showing various alas basins and lakes; compiled by Mathias Ulrich (Spot Satellite, 25.09.2012)

*Figure 3 - Field impressions: a: drained lake basin in the northern part of the Yukechi Alas in summer; b: drained lake basin in the Yukechi Alas in winter; c: drilling in the alas center (**Alas1**); pictures by Mathias Ulrich (a), Jens Strauss (b & c)*

2.1 Local and regional geomorphology

The Lena-Aldan interfluve, located in Yakutia, is a large basin ranging in elevation from approx. 130 m above sea level (asl) in the river valleys to approx. 400 m asl at mountain tops. The study site itself is 200 to 220 m asl and is part of the south-western marginal zone of the Abalakh erosion-constructional plain (Fedorov et al., 1998) and is already part of the erosional slope of the terrace (personal communication Christine Siegert). The main relief characteristics in the Yukechi Alas area are flat plains

and thermokarst lakes of up to four metres depth (**Figure 3**). New basins are forming continuously through active thermokarst processes that are naturally, as well as anthropogenically induced (Fedorov and Konstantinov, 2003). Also, the presence of seasonally flooded river basins is due to the Lena River. The Lena River is the main water resource in the Yakutsk area, because permafrost conditions prevent ground water upwelling away from the river.

2.2 Climate and climate history

Central Yakutia is characterized by an humid, extreme continental climate regime with very low winter temperatures (Köppen and Geiger, 1930). Winters are six months long with little snow fall and air temperatures often reach lows of < -60 °C. The highest temperatures occur in July (30 - 33 °C). Climate records show temperatures averaged over 30 years (1961 to 1990 and continuously modelled afterwards) ranging from -41 to 18 °C, giving an annual mean temperature of -10.2 °C and a mean amplitude of 59 °C (**Figure 4**). For the same period, the mean annual precipitation was 246 mm in Yakutsk at 133 m asl. The precipitation ranged from 6 mm in March to 40 mm in (**Figure 4**).

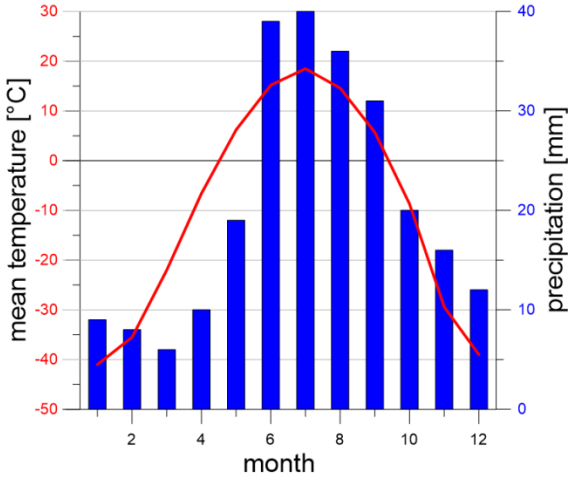

Figure 4 - Climate diagram for Yakutsk, Yakutia, Russia (Skålin and Norwegian Meteorological Institute, 2018)*; altitude: 133 m asl, mean annual temperature: -10.2 °C, annual precipitation: 246 mm/a; humid, continental climate (Köppen and Geiger, 1930)*

Holocene climate reconstructions in this region indicate climate settings with similar or slightly colder conditions or slightly colder, with summer temperatures around 15.6 °C (Hubberten et al., 2004; Nazarova et al., 2013; Ulrich et al., 2017).

2.3 Permafrost conditions

As Central Yakutia is located in the continuous permafrost zone, periglacial processes are one of the major features of landscape evolution. At the study site, several thermokarst lakes were found, some of which recently drained. The Yedoma Ice Complex and refrozen alas terrain are found in this area, as well as taliks below lake bottoms with sufficiently deep water. Recent studies (citation) show that warming air temperatures in Central Yakutia lead to greater thaw depths and talik development. Similar observations were made at the study site for this project. Permafrost in this area is in a dynamic state due to ground subsidence caused by temperature disturbances. Ground ice is found in shallow depths of approx. 2 m in Central Yakutia, with an active layer thickness of ~ 1.5 m (Fedorov, 2006). The active layer thickness ranges from 200 cm in alas basin grasslands to 100 cm in the boreal forest (personal communication J. Strauss, Mathias Ulrich). During the field work period, the active layer was frozen.

2.4 Flora and fauna

Most of Central Yakutia is covered with taiga and larch forest, mainly consisting of *Larix cajanderi*, *Larix gmelinii*, *Larix sibirica* and *Larix czekanowskii* with several *Pinus sylvestris* communities (Troeva et al., 2010; Desyatkin et al., 2014). The Yukechi Alas is covered with grassland (**Figure 3**) dominated by steppe and bog plant species and surrounded by boreal forest (**Figure 3**) (Ulrich et al., 2017).

These grasslands are often extensively used for pasture so different cattle species are among the most influential fauna (Katamura et al., 2006). Also *Alces alces* and *Ursus arctos* are common.

3 Methods

3.1 Field work

Field work took place in March 2015 during a joint expedition of Alfred Wegener Institute for Polar and Marine Research, University of Leipzig and the Melnikov Permafrost Institute, Siberian Branch of Russian Academy of Sciences. The field work was part of the ERC project "Rapid Permafrost Thawing in a Warming Arctic and Impacts on the Soil Organic Carbon Pool (PETA-CARB)" as well as the DFG project "Short and long-term thermokarst dynamics due to climate changes and human impacts in Central Yakutia, Siberia (2013-2016)". In total four cores (two alas cores and two Yedoma cores) were drilled (**Figure 3**), each approx. 20 m in depth. Due to partially unfrozen permafrost conditions within the cores, sections of the cores were lost during drilling. Two of four cores were analysed in this study: one Yedoma core (YUK15-YED1), 22.35 m length, and one alas core (YUK15-Alas1), which is 19.80 m in depth and contains a larger talik from approx. 1.6 down to 7.5 m (**Figure 5**; **Figure 6; Figure 7**). Both, YED1 core and Alas1 core, were drilled from dry surface, while the remaining two were drilled at the bottom of thermokarst lakes.

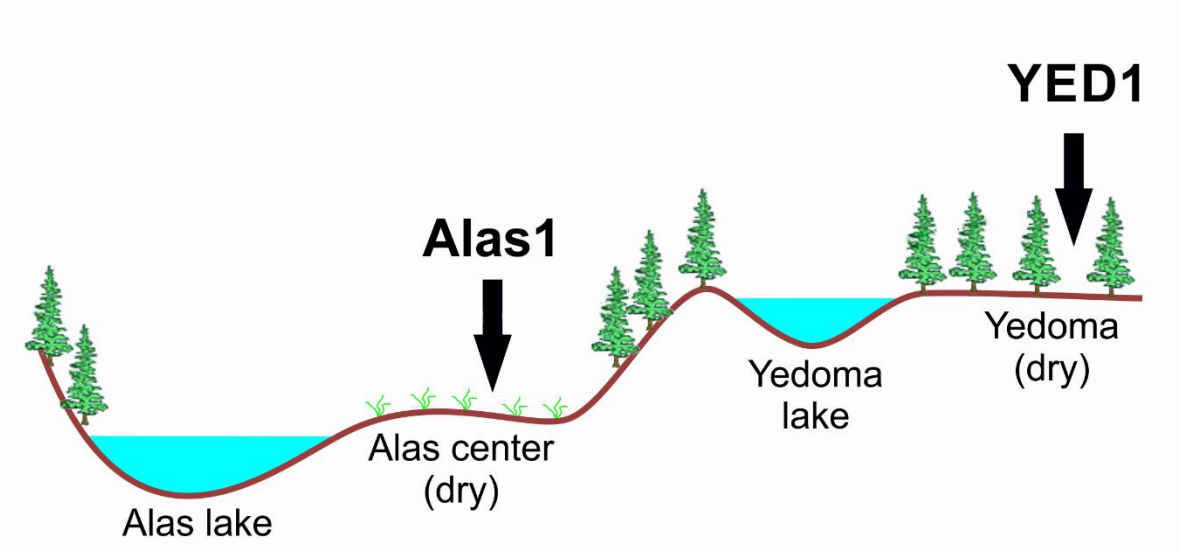

Figure 5 - Drilling locations in the Yukechi Alas landscape, roughly depicting the predominant vegetation types at the sites and their location relative to the lakes (picture by Jens Strauss)

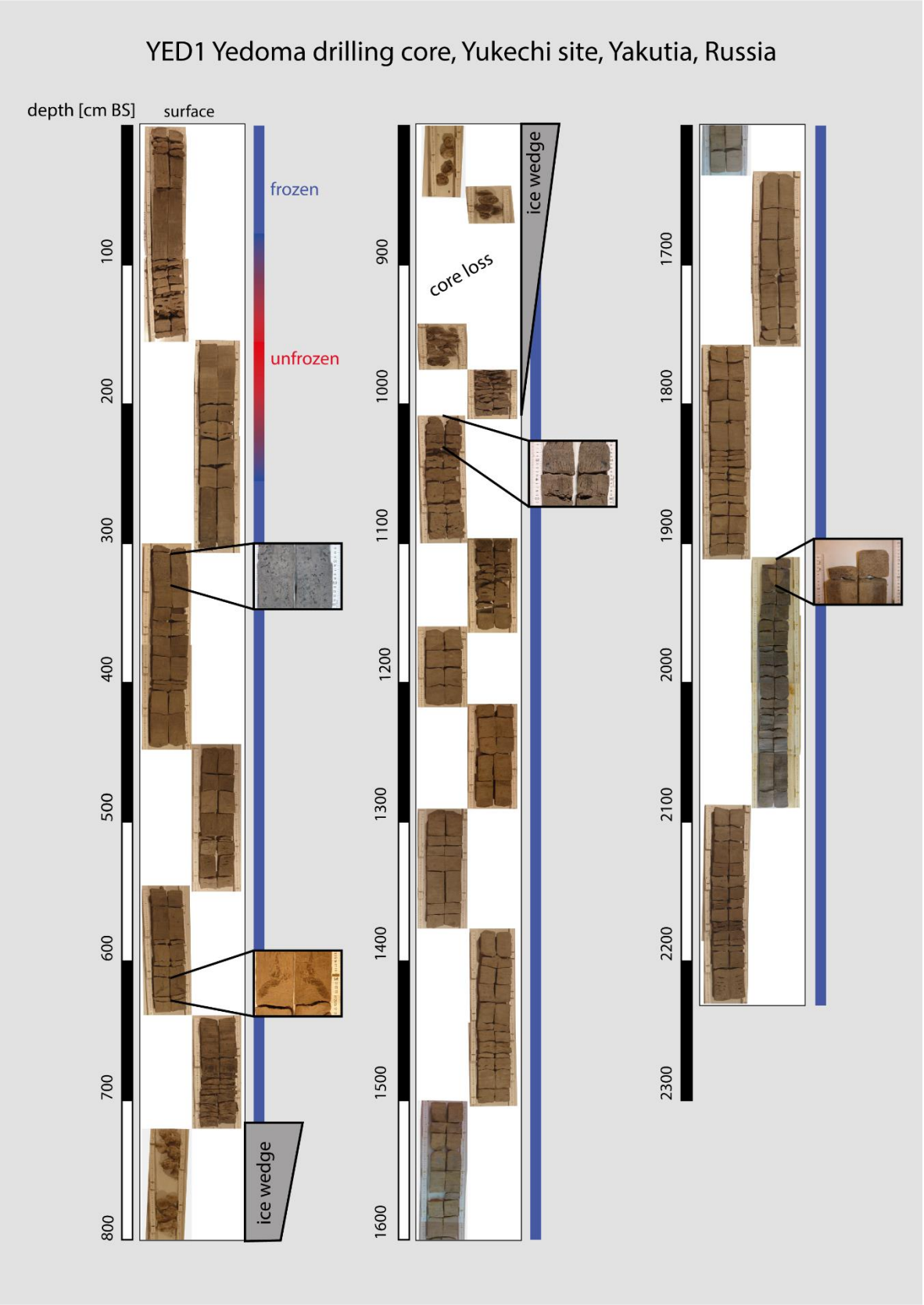

Figure 6 - YED1 drilling core; core profile showing the state of the core sections; close-ups show main cryostructures

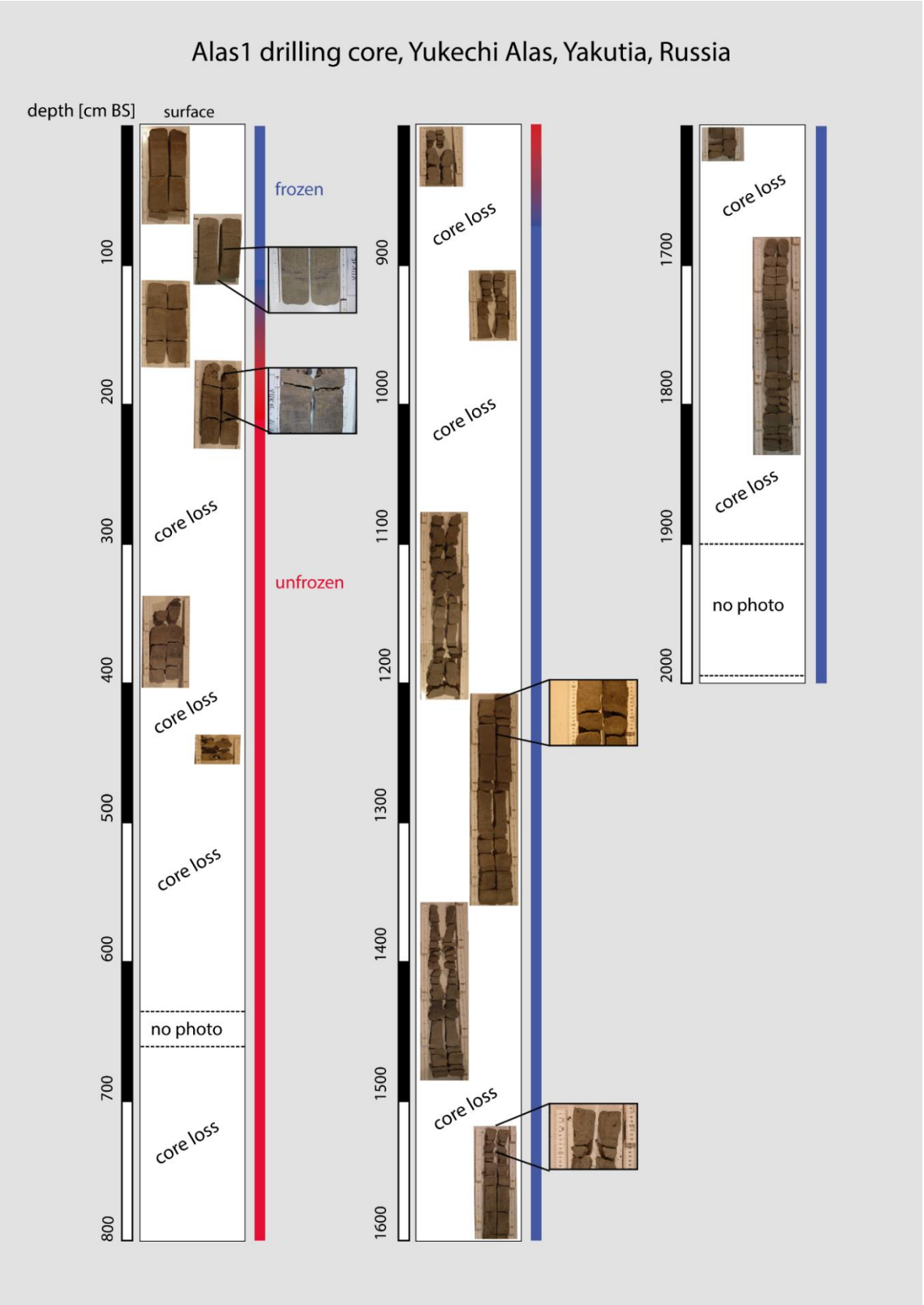

Figure 7 - Alas1 drilling core; core profile showing the state of the core sections; close-ups show main cryostructures

3.2 Laboratory work

To determine the characteristics of the deposits in terms of carbon content and sources, sediment characteristics and sedimentary history, cryogenic structures, local permafrost formation and the permafrost's carbon storage capacity, measurements was carried out on subsamples obtained from each core. The samples were analysed for ice content, total carbon (TC), total organic carbon (TOC) and total nitrogen (TN) content, isotopic abundance ratio of total organic carbon ($\delta^{13}C$ of TOC), grain size and mass specific magnetic susceptibility. Radiocarbon dating was applied to 9 equally distributed samples. The porewater of each sample were analysed for pH, electric conductivity, dissolved organic carbon (DOC) and isotope abundance ratios of oxygen ($\delta^{18}O$) and hydrogen ($\delta^{2}H$).

3.2.1 Sample preparation

To subsample the still-frozen cores, each core was split lengthwise at -10 °C in the climate chamber of GFZ Potsdam, using a Makita band saw. First these halves were cleaned, photographed and cryolithologically described. One of the obtained halves was kept intact as an archive piece, while the other half was sawn into approx. 5 cm long sample pieces at the selected subsampling depths. These were selected equally distributed along the cores every approx. 50 cm with shifts due to cover the majorstratigraphical layers. In total 64 samples were selected.

All samples were weighted for subsequent moisture content analyses.

3.2.2 Water sample extraction

To analyse the frozen water inside the samples for pH, conductivity, dissolved organic carbon (DOC), oxygen isotopes ($\delta^{18}O$ – ratio) and hydrogen isotopes ($\delta^{2}H$ – ratio), the samples were thawed at +4 °C. Rhizones, which represent artificial plant roots, were inserted into the thawed sample. Rhizones (RHIZON MOM 10 cm, Rhizosphere Research Products) consist of a porous PE/PVC tube, strengthened by glass fiber, with a diameter of 2.5 mm. A vacuum was applied using syringes, the latter of which were used as short-term storages as well. The contents of the syringes were then distributed into several subsample containers. The DOC subsamples were then acidified using 20 µl concentrated (35 %) hydrochloric acid (HCl) to preserve the sample for later analysis. The leftovers were frozen as backup samples.

Due to low ice contents as well as small sample amounts in some cases, not all samples could be analysed for all named parameters.

Oxygen and hydrogen isotope abundance ratios will be included in this study to gain insight on environmental conditions during ice formation (**table 2** and **4**).

3.2.3 Stable oxygen and hydrogen isotopes

Due to the different physical properties of hydrogen and oxygen isotopes, precipitation and evaporation have an impact on isotope composition of ice found in permafrost. Lighter isotopes evaporate more easily and are therefore found in greater amounts in seasonal, quickly freezing water, while heavier isotopes remain in snow layers during melting, seeping into the active layer forming e. g. ice wedges.

To determine the ratios of $^{2}H/^{1}H$ and $^{18}O/^{16}O$, samples were measured using a Finnigan MAT Delta-S mass spectrometer and the equilibration technique after Horita (Horita et al., 1989; Meyer et al., 2000).

Following Meyer et al. 2000, 5 ml per sample were filled into 25 ml glass bottles and inserted into stirred water baths to induce a homogenous temperature (18 ± 0.01 °C). Subsequently they were evacuated, and the gases were equilibrated between water and H_2 gas for $\delta^{2}H$, using activated platinum as a catalyst. The same procedure was repeated for $\delta^{18}O$ measurement using CO_2 and water

for equilibration. A laboratory internal standard SEZ (Severnaja Zemlja water) was used for quality control.

After equilibration, the gas was separated from the water by freezing the bottles at -78 °C and transferred into the sample bellow. In alternation, sample gas and reference gas were lead into the mass spectrometer. Ten measurements per sample at 5 nano Amperes (nA) H_2 for δ^2H and at 10 nA mass 44 intensity for $\delta^{18}O$ were carried out. Internal errors were better than 0.8 ‰ for δ^2H and better than 0.1 ‰ for $\delta^{18}O$.

3.2.4 Ice content determination

Determination of the samples' ice content was carried out by freeze-drying the pre-weighted samples. For this, the re-frozen samples were left in their opened bags and jars and covered with a thin layer of tissues to prevent dust and fine particles from being lost during the drying process. They were then put into a Zirbus Subliminator 3-4-5 at approx. 0.2 bar and -40 °C for at least 48 hours to remove any moisture contained. In the following the samples were weighted again to determine the ice content in wt% (**Equation 1**).

(1) $$absolute\ ice\ content\ [wt\%] = \frac{wet\ weight\ [g] - dry\ weight\ [g]}{wet\ weight\ [g]}$$

The ice contents of the samples are shown in **tables 1** and **3**.

3.2.5 Sample division

Using forceps and spatula, the dried samples were homogenised and split into subsamples for MS and GSA, element analysis of TC, TOC and TN, XRF (not included in this study) analysis, biomarkers (not included in this study) and an unaltered archive sample. Subsamples for radiocarbon dating were taken for 9 samples during this process.

The subsamples taken for element analysis were powdered using a Fritsch pulverisette 5 planetary mill equipped with agate jars and agate marbles. Each sample was milled for 8 minutes at 360 rotations per minute. The samples are transferred into plastic jars using a brush and spatula.

3.2.6 Radiocarbon dating

For radiocarbon dating, subsamples of bulk material were taken out of the selected 9 samples during division. Dating took place at AWI Bremerhaven using a **Mi**ni **Ca**rbon **Da**ting **S**ystem (MICADAS). Ages were calibrated using Calib 7.1 (Stuiver et al., 2018), and the age-depth-model was developed using the Bacon package in the R environment version 3.3.1 (Blaauw and Christen, 2011; R Core Team, 2016). For calibration (calibrated years before present (cal yr BP)), IntCal13 was used (Reimer et al., 2013).

3.2.8 Total carbon (TC) and total nitrogen (TN) determination

All ground samples were measured twice for TC and TN combined using 5 to 5.8 mg of each sample per measurement. The weigh-in was carried out using a Sartorius micro M2P laboratory scale with an accuracy of ± 0.001 mg. Samples were put into pure tin capsules and tungsten(VI)oxide was added for combustion catalysis. Analysis was carried out by using an vario EL III Element Analyzer (Elementar Analysensysteme GmbH), which first heats up the samples until 950 °C within an oxygen-saturated helium atmosphere. Carbon dioxide (CO_2), elemental nitrogen (N_2), nitrogen oxide (NO) and nitrogen dioxide (NO_2) are formed and then reduced inside a copper-filled reduction tube at 850 °C.

Analysis then starts at 50 °C when nitrogen is mobilized and transfers into the measurement chamber, getting detected by a heat conductivity sensor, resulting in a peak in heat conductivity. The vario EL III then heats up to 130 °C, allowing for carbon dioxide to reach the measuring chamber, resulting in another heat conductivity peak. Height and expansion of these peaks are put into context with initial

sample weight, giving TC and TN values in wt% with an accuracy of 99.9 % for nitrogen and 99.95 % for carbon.

To prove these accuracies, an initial set of calibration standards, consisting of acetanilide, sucrose and 30 % EDTA, was measured, as well as a control sequence of 20 % EDTA, 12 % calcium carbonate, IVA33802150 (soil standard, C=6.7 %, N=0.5 %, S=1.0 %), soil standard 1 (C=3.5 %, N= 0.216 %) and S/N 338 40025 (soil standard, C=1.697 %, N=0.186 %) in between each 30 measurements. Each sample was measured twice and the lab internal difference between the two measurements is 10 % maximum.

3.2.9 Total organic carbon (TOC) determination

To differentiate between TC and TOC, all samples were measured with an elementary analysis device varioMAX C Element Analyzer (Elementar Analysensysteme GmbH). It uses catalytic tube pyrolysis with pure nitrogen (99.996 %) as a carrier gas. Sample mass for this measurement depends on its TC content and the samples were weighted into steel crucibles accordingly, using a Mettler Toledo XS105 dualrange analysis scale (accuracy of ± 0.1 mg).

Prior to a sample measurement, a calibration set was measured consisting of 30 % glutamate, pure glutamate and 2:3 glutamate. A control sequence after each 15 samples was made up of 2:3 glutamate, 10:40 glutamate, 5:45 glutamate and 1:19 glutamate.

The crucibles containing the samples were heated to 580 °C in an oxygen-saturated helium atmosphere, resulting in carbon dioxide formation. The gases were then further heated until 930 °C to ensure the complete carbon dioxide formation from all present organic carbon. The varioMAX C Element Analyzer is equipped with two detection tubes, where one is used for samples with little carbon content up to 2 % and therefore is more sensitive, while the other is used for samples containing more than 2 % of carbon. However, there is a minimum detectable carbon content of 0.1 %. To determine the carbon dioxide peak during integration, the cut off value is calculated from parameters such as sample mass and expected carbon content. The value and occurrence time of this peak enable the determination of the total amount of organic carbon. The accuracy of the measurement was 99.9 %. To gain information about the decomposition state of the organic matter in the samples, a ratio was calculated from TOC and TN values, referred to as C/N. A higher ratio indicates a better-preserved state of the contained organic matter.

3.2.10 Stabile carbon isotopes

To prepare the samples for stabile isotope analysis, any carbonate ions present had to be removed. In order to do so, a small amount of each sample was heated to 97.7 °C for three hours in 20 ml 1.3 molar hydrochloric acid (HCl) in 100 ml Erlenmeyer glass flasks and diluted with purified water afterwards. During cooking, the reaction expressed in **equation 2** took place.

To remove the Cl^- ions originating from the hydrochloric acid, dilution and sedimentation were repeated until Cl^- content was less than 500 ppm. This was to ensure pure isotope measurement, as charged ions would influence the electromagnetic field in the following mass spectrometry measurements as well as react different to ionization. To test for the Cl^- content, Quantofix Chloride test stripes were used. The diluted samples were vacuum-filtrated using GE Healthcare Life Sciences Whatman glass microfiber filters, dried at approx. 50 °C afterwards and subsequently grinded by hand.

The preparation of the measurement involved placing each sample in pure tin capsules with a targeted weight following **equation 3**. The weigh-in was carried out using a Sartorius micro M2P (accuracy of ± 0.001 mg) with a deviation of 0.02 mg maximum in reference to the target weight. The analysis was carried out using a Delta V Advantage Isotope Ratio MS supplement (Thermo Fisher Scientific) equipped with a Flash 2000 Organic Elementar Analyzer (Thermo Fisher Scientific), which both use pure helium for carrier gas.

The analysis consists of a number of steps, starting with sample combustion and oxidation at 1020 °C with chrome dioxide (CrO_2) as an oxidant. This leads to the formation of carbon dioxide (CO_2) and several nitrogen oxides (NO_x). They were then reduced at 650 °C using elemental copper (Cu), forming pure nitrogen (N_2), but leaving the CO_2 unaltered. Separation of these gases is realized by use of a gas chromatography tube, which is faster passed by the lighter nitrogen molecules than the heavier CO_2. Therefore, nitrogen enters the mass spectrometry unit earlier. In there, elemental nitrogen from an external source is measured as reference, followed by the nitrogen partition of the sample. Once nitrogen has passed through the unit, the sample's CO_2 partition reaches the mass spectrometer and is followed by external CO_2 for a reference measurement. Measuring works by ionizing the sample or reference gas by inducing energy via electron impulses. The analysis unit then separates the ions following the sample's mass/charge ratio and detects the ions' energy intensity at the detection unit. The measured values got linearly corrected using the reference measurements. The accuracy of this measurements was ± 0.15 ‰.

(2) $CO_3^{2-} + 2HCl \rightarrow CO_2 + 2\,Cl^- + H_2O$

(3) $target\ weight\ [mg] = \frac{20}{TOC\ [wt\%]}$

$\delta^{13}C$ measurements were carried out for 23 out of 64 samples as it requires detectable TOC amounts, which only 23 samples provided (see **tables 2** and **4**).

Values for $\delta^{13}C$ are calculated in ‰VPDB (artificial standard, Vienna Peedee Belemnite).

Measurement values are negative as the VPDB reference value has a very high C^{13}/C^{12} ratio (Coplen et al., 2006) and were corrected for plotting using $|\delta^{13}C|$**.**

3.2.11 Mass specific magnetic susceptibility

Magnetic susceptibility (X_m) was measured using a Bartington Magnetic Susceptibility Meter Model MS2, equipped with a Bartington Magnetic Susceptibility Sensor MS 2B (Bartington Instruments, UK). It measures the magnetizability of a sample in an external magnetic field in 10^{-8} m^3 kg^{-1}. The magnetic field varies sinusoidally, depending on the set frequency. Frequences used for measurement were 4.65 kHz (high) and 0.465 kHz (low).

Due to large differences, three groups of minerals can be differentiated by this: diamagnetics (e.g. quartz, feldspar), paramagnetics (e.g. pyroxene, biotite) and ferro- and ferrimagnetics (e.g. magnetite, iron sulfides). While diamagnetics do not have a magnetic dipole moment, paramagnetics have a permanent dipole which is excited by activating the external magnetic field. Ferromagnetics show an own permanent magnetic dipole, hence they are slightly magnetic without being externally magnetized, which gets stronger by using the external field (Butler, 1992; Dearing, 1999).

X_m is a mass specific parameter, defined as the ratio of volume magnetic susceptibility (κ) and the bulk density (ρ). This is shown in **equation 4**. The MS2 can directly measure X_m, but for calibration each sample was measured three times and the average was calculated.

(4) $X = \frac{\kappa}{\rho}$

3.2.12 Grain size analyses

In preparation for grain size analyses, organic matter contained in the samples was removed. To do so, the grain size subsamples were treated with 100 ml 3% hydrogen peroxide (H_2O_2) and approx. 4 ml 25% ammonia. The samples were then put on a shaker for 28 days to allow for all organic matter to react. To maintain a reaction-supporting pH between 6 and 8, small amounts of 25% ammonia or concentrated acetic acid were added, after adding 10 ml 30% hydrogen peroxide (H_2O_2).

Grain size distribution was measured using a Malvern Mastersizer 3000 (Malvern Instruments, UK) equipped with a Malvern Hydro LV wet-sample dispersion unit. This device uses a red 633 nm laser and a blue 470 nm LED, which are sent into the suspended samples and their refraction is measured by a focal and several scatter light detectors, which detect the light scattering for each particle. The light impulses on each detector are used to calculate the contained grain sizes.

To optimize the results, the organic-free samples underwent another series of preparation steps. First they were filled up with purified water and centrifuged to narrow the sample volume. Subsequently, the samples were freeze-dried and homogenized. 1 g of each sample was then weighted into plastic jars, mixed with approx. 0.5 g tetra-Sodium Pyrophosphate 10-hydrate ($Na_4P_2O_7*10H_2O$) for dispersion and 0.0001 % ammonia solution and put on a Gerhardt Laboshake overhead shaker for at least 24 hours.

The resulting samples were divided into eight equal subsamples using a Fritsch laborette 27 Rotary Sample Divider. Each one of them was measured using the Mastersizer, which resulted in three measurements per subsample. If deviation in small, middle and large grain size classes was less than 10 % after measuring three subsamples, these results were taken as representative for the whole sample. Otherwise, measurement was continued, until the whole set of eight subsamples was measured. In the following, an averaged record is created per sample, consisting of the values of the several subsample measurements.

All statistics were calculated out of these measurements using Gradistat (Blott and Pye, 2001).

Results are shown in **tables 1** and **3**.

For grain size classification, the international ISO 14688-1:2017 scale was used, classifying clay as particles ≤ 2 µm, silt ranging from 2 to 63 µm and sand ranging from 63 µm to 2 mm (ISO, EN, 2017), while all particles > 1 mm were removed during the sample division process; no particles > 1 mm were found.

All graphs were plotted using Grapher (Golden Software, LLC.), if not specified.

4 Results

4.1 Core description

The YED1 core appears optically heterogenous with material varying from fine clayish grey material to sandy greyish brown material. The ground ice types include structureless to micro-lenticular ice, as well as larger ice veins and bands (highlighted in **Figure 6** at 620 and 1030 cm BS). An ice wedge was found ranging from 691 to 1005 cm BS (**Figure 6**) and is represented by fractioned pieces of ice in the core. Seemingly organic matter is visible in form of brown to black dots and lenses up to 2 cm in diameter (highlighted in **Figure 6** at 330 cm BS). Parts of an adjacent sand wedge were found at 1920 cm BS (**Figure 6**). It contains one talik close to the surface at approx. 100 to 200 cm BS.

*Figure 8 - YED1 core 1333-1345 cm BS; representative picture for the third unit (sandy) (**Figure 9**) of the YED1 core with micro-lenticular to non-visible ice; left ruler: continuous depth measurement, right ruler: location within the core fractal examined*

Figure 8 displays the appearance of the YED1 core between approx. 1000 and 1900 cm BS representatively. It has a light, greyish colour and a coarse texture without any visible ice. There are no optically organic-rich areas visible in this fraction of the core. This matches the laboratory results of very low ice content and sandy material with no detectable carbon (**Figure 9**).

Large sections of the Alas1 core were lost during drilling because a talik was encountered (approx. 160 to 750 cm BS). It appears to be more homogenous than the YED1 core in terms of colours and material (clayish to silty greyish brown material) (**Figure 7**). Ice structures are mostly horizontal ice lenses up to 5 cm thick and structureless non-visible ice. Organic matter is present in the form of blackish dots and lenses up to 1 cm in diameter (highlighted in **Figure 7** at 1530 cm BS).

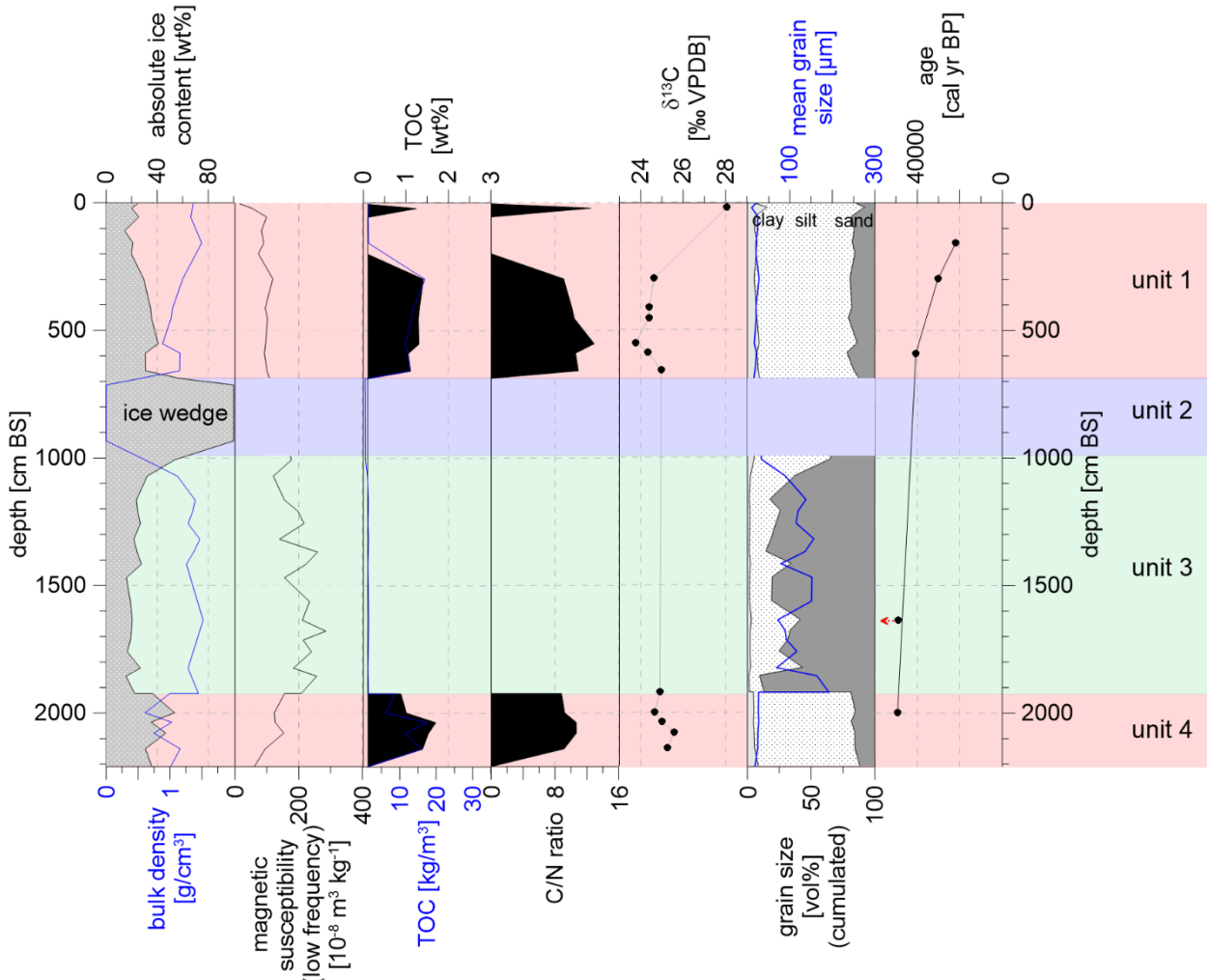

*Figure 9 - Laboratory results of **YED1** (ice content, bulk density, magnetic susceptibility, TOC, C/N, $\delta^{13}C$, grain size, ages); red arrow indicates an infinite carbon age*

4.2 Sedimentology

Laboratory results of the absolute ice content, the low-frequent magnetic susceptibility, TOC, C/N ratio, $\delta^{13}C$ and cumulated grain size distribution were plotted over depth for both cores YED1 (**Figure 9**) and Alas1 (**Figure 10**). For plotting, the mean sample depth was used (**Tables 1** and **3**). Measurement results are listed in **tables 1** & **2** (YED1), **3** & **4** (Alas1) and **5** (carbon dating).

YED1 can be divided into four main units (**Figure 9**). Unit 1 with similar ice content, magnetic susceptibility and grain size distribution ranges from the top down to approx. 700 cm BS, where the ice wedge begins. Unit 2 represents the ice wedge down to approx. 1000 cm BS. Unit 3 shows smaller ice content and higher sand content than the other units and does not contain carbon. Finally, unit 4, starting at approx. 1920 cm BS, is very similar to unit 1 with slightly higher ice content.

Ice content within talik areas (**Figures 6** and **7**) represents water content, which froze after drilling.

Bulk density follows the exact opposite path of ice content (**Figure 9**), ranging from 0.54 g/cm^3 (688 cm BS) to 1.52 g/cm^3 (1636 cm BS). As ice (or water) content decreases, more sediment is present in same sample volumes. The calculated bulk density for the ice core (ice content = 100 vol%) is zero.

The ice content appears stable within each unit with smallest ice content throughout unit 3 (**Figure 9**), varying between 14.6 and 57.4 wt% with an increase towards the ice wedge (unit 2) and in the bottom zone (unit 4).

Magnetic susceptibility shows a general increase with depth (**Figure 9**), ranging from 15.4 * 10^{-8} m^3 kg^{-1} at the surface to 285 * 10^{-8} m^3 kg^{-1} at 1679 cm BS and decreasing below. Unit 3 shows generally higher values than the other units. The values within the ice wedge are graphically interpolated, linking the above- and below- ice wedge values. Within the general increase, magnetic susceptibility values are unsteady in unit 3 and slightly decrease in unit 4.

TOC values reach detection limit (0.1 wt%) in 12 samples (**Figure 9**). All values below detection limit are set as 0.1 wt% for plotting. Detectable values range from 1.1 wt% (589.5 cm BS) to 1.7 wt% (2036 cm BS). TOC density follows the TOC share, ranging from 0.61 kg/m^3 (1007.5 cm BS) to 17.5 kg/m^3 (2036 cm BS).

Both TOC and TN values often are below detection limit (0.1 wt% for TOC, TN), which does not allow for C/N calculation for samples with either TOC or TN below detection limit. TN values range from 0.101 wt% to 0.16 wt% in samples above detection limit (n= 9), which allowed for calculation of 12 C/N values (**Figure 9**). If both TN and TOC were less than 0.1wt%, no C/N ratio was calculated. The C/N values correlate with the TOC values. The range is 9.1 (298 cm BS) to 12.9 (552.5 cm BS).

In $\delta^{13}C$, the sample closest to the surface (21 cm BS) has a value of -28.07 ‰VPDB, all remaining samples range from -23.78 ‰VPDB (552.5 cm BS) to -25.57 ‰VPDB (2078.5 cm BS) (**Figure 9**).

Grain sizes are plotted cumulatively (**Figures 9**, **15** and **16**) and clearly display differences between the different fractions. In unit 1, silt is the dominant grain size. Both, silt and clay content decrease in unit 3 while sand increases. In unit 4, grain size distribution is once again dominated by silt, similar to unit 1.

The mean grain size matches the changes in volumetric share of the different grain size fractions.

The carbon ages show a decreasing steepness towards the surface. The value marked with a red arrow (1636 cm BS) represents an infinite age. The oldest sample with an age of 49 323 cal yr BP is at 1998.5 cm BS while the youngest sample is 21 890 cal yr BP at 157.5 cm BS (**Figure 9**).

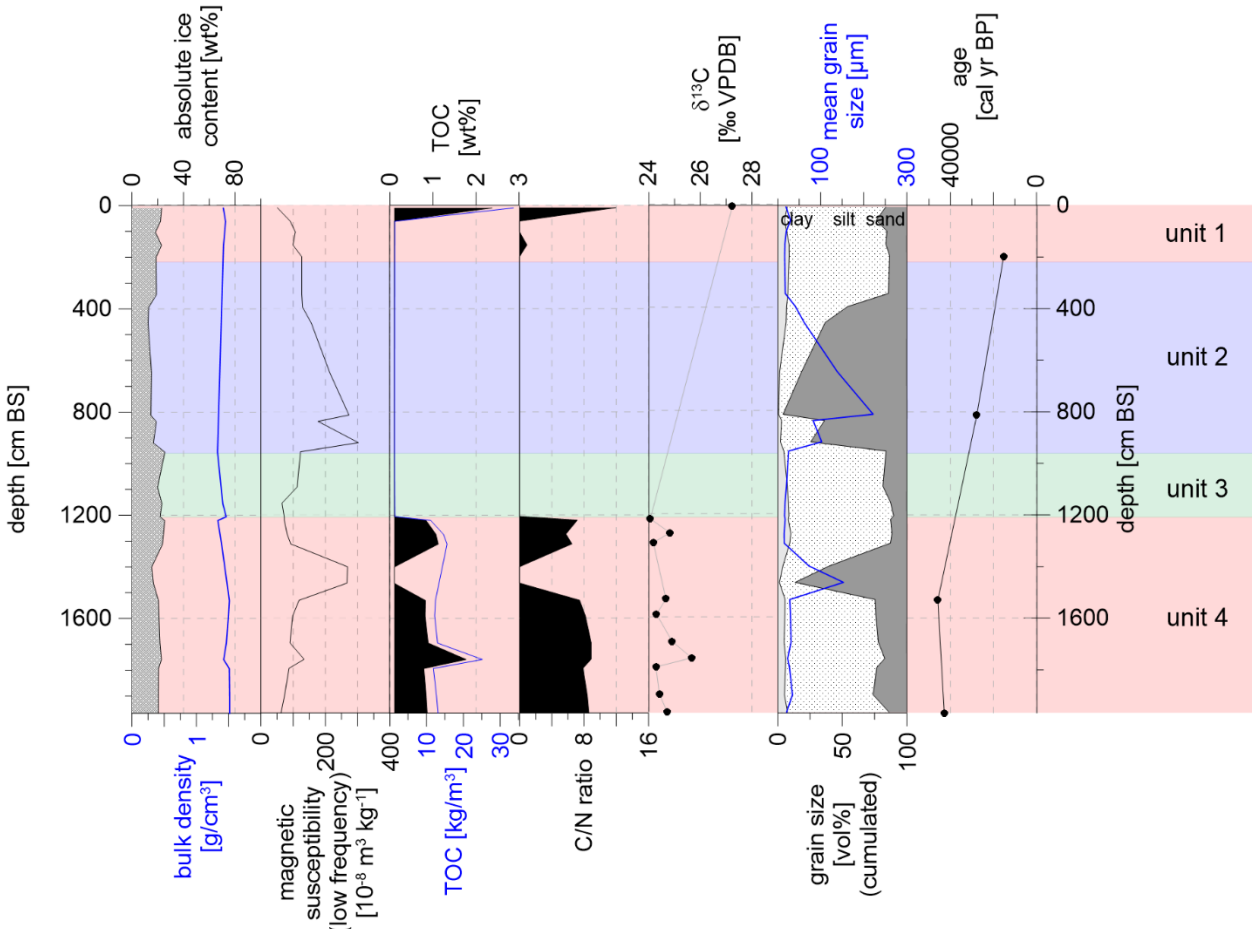

*Figure 10 - Laboratory results of **Alas1** (ice content, bulk density, magnetic susceptibility, TOC, C/N, δ13C, grain size, ages)*

As YED1, Alas1 is also characterized by four main units (unit 1: 0 to approx. 220 cm BS, unit 2: 220 to approx. 980 cm BS, unit 3: 980 to approx. 1230 cm BS, unit 4: 1230 cm BS to bottom).

In the Alas1 core, in direction from top to bottom, ice content (**Figure 10**) first drops (23.1 wt% to 12.5 wt%) rises peak-like to 25.6, drops again and finally becomes steady around 21 wt%

Bulk density appears steady around 1.5 g/cm^3 with slightly smaller values in unit 3 and the upper part of unit 4 (**Figure 10**).

Magnetic susceptibility follows the opposite pattern (**Figure 10**), as it first rises throughout units 1 and 2 (50.772 * 10^{-8} m^3 kg^{-1} at 9 cm BS to 302.377 * 10^{-8} m^3 kg^{-1} at 919.5 cm) with a single sharp drop before the peak, down to 177.118 * 10^{-8} m^3 kg^{-1} at 837 cm BS. Then, it decreases further, in unit 3 down to 65.358 * 10^{-8} m^3 kg^{-1}, but then increases sharply to another peak at 1400.5 cm BS with a value of 268.690* 10^{-8} m^3 kg^{-1}. After this point, it continuously decreases until 62.146 * 10^{-8} m^3 kg^{-1} (unit 4).

TOC measurement for 11 samples are plotted versus depth (**Figure 10**). They show a peak of 2.4 wt% at the top sample (9 cm BS) followed by 1207 cm (15 samples) below detection limit (units 2 and 3). Values peak again at 1.12 wt% at 1312 cm BS, drop below detection limit and then rise to a steady phase around 0.8 wt% for 437 cm with a single sharp peak of 1.8 wt% at 1759 cm BS.

TOC density aligns with the TOC share but does not duplicate the negative peak found in TOC share at 1470 cm BS. Values range between 1.33 kg/m^3 (955 cm BS) and 33.6 kg/m^3 (9 cm BS) (**Figure 10**).

C/N values follow a similar pattern (**Figure 10**) as detectable amounts of TN were only present within samples with detectable TOC, except for the sample at 153.5 cm BS that contained 0.11 wt% nitrogen

but no detectable TOC. C/N values show a sharp peak at the surface (12.0 at 9 cm BS), a single value of 0.9 at the exceptional TN sample and continue with undetectable values down to 1220 cm BS where they reach a value of 7.2. The values drop again below detection limit and then enter a steady phase around 8 reaching from 1530.5 cm BS down to the bottom. The minimum C/N ratio is 0.9 at 153.5 cm BS, the maximum value is found near the surface with 12.0 (9 cm BS).

$\delta^{13}C$ values range from -24.06 ‰VPDB to -27.24 ‰VPDB near the surface (9 cm BS) (**Figure 10**). In the rest of unit 1 as well as in units 2 and 3, no values re available. In unit 4, values scatter between -24.06 ‰VPDB (1220 cm BS) and -25.67 ‰VPDB (1759 cm BS).

The grain size distribution (**Figure 10**) shows two peaks in the sand fraction in unit 2 (96.0 vol% and 81.4 vol%). Low but steady sand contents are found from top down to 344.5 cm BS (13.3 to 23.7 vol%). Units 3 and 4 show similar sand content with an exception at 1400.5 cm BS. Clay content falls down to 0.7 vol% at the first sand peak in unit 2 and reaches its maximum at the top of unit 4. Silt content increases as sand content falls, following the steady phases with values varying between 71.0 and 77.8 vol% (top to 344.5 cm BS), 74.0 and 81.1 vol% (955 to 1312 cm BS) and 68.7 and 78.7 vol% (1530 to 1967.5 cm BS). The minimum silt content is found along the maximum sand content at 812.5 cm BS (3.4 vol%). The maximum silt content is 81.1 vol% at 1205.5 cm BS.

The calibrated carbon ages show an age inversion at 1530.5 cm BS and a rather continuous steepness. The deepest sample has a carbon age of 42 865 cal yr BP while the uppermost sample is approx. 15 287 cal yr BP (**Figure 10**).

There is a peak present throughout most parameters at approx. 1470 cm BS with high magnetic susceptibility and sand content combined with low carbon and ice content.

4.2 Carbon characteristics

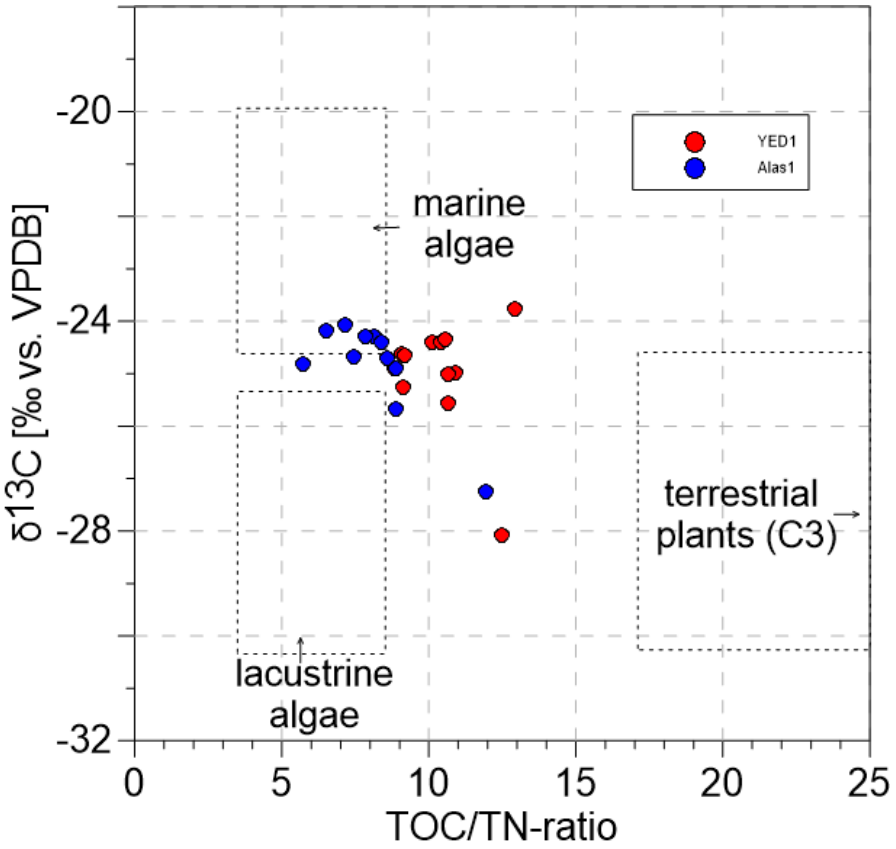

Figure 11 - C/N - $\delta^{13}C$ plot showing the origin of carbon (Meyers, 1997)

In **figure 11**, the TOC/TN or C/N ratio was plotted against the $\delta^{13}C$ values for both YED1 (red, **Figure 11**) and Alas1 (blue, **Figure 11**) core.

Both cores show a dense distribution, whereas the YED1 core has generally higher C/N values compared to Alas1. $\delta^{13}C$ values are similar for both cores. Each of the cores has one outlier close to the surface with higher C/N and lower $\delta^{13}C$ values (4 cm BS for YED1, 9 cm BS for Alas1).

Those surface samples therefore show a more terrestrial (C3 plants) characteristics compared to the rather aquatic or lacustrine algae dominated signal of the other samples. The samples taken from YED1 show a weaker lacustrine signal or higher share of terrestrial material than the Alas1 samples (**Figure 11**).

4.3 Water isotope signature

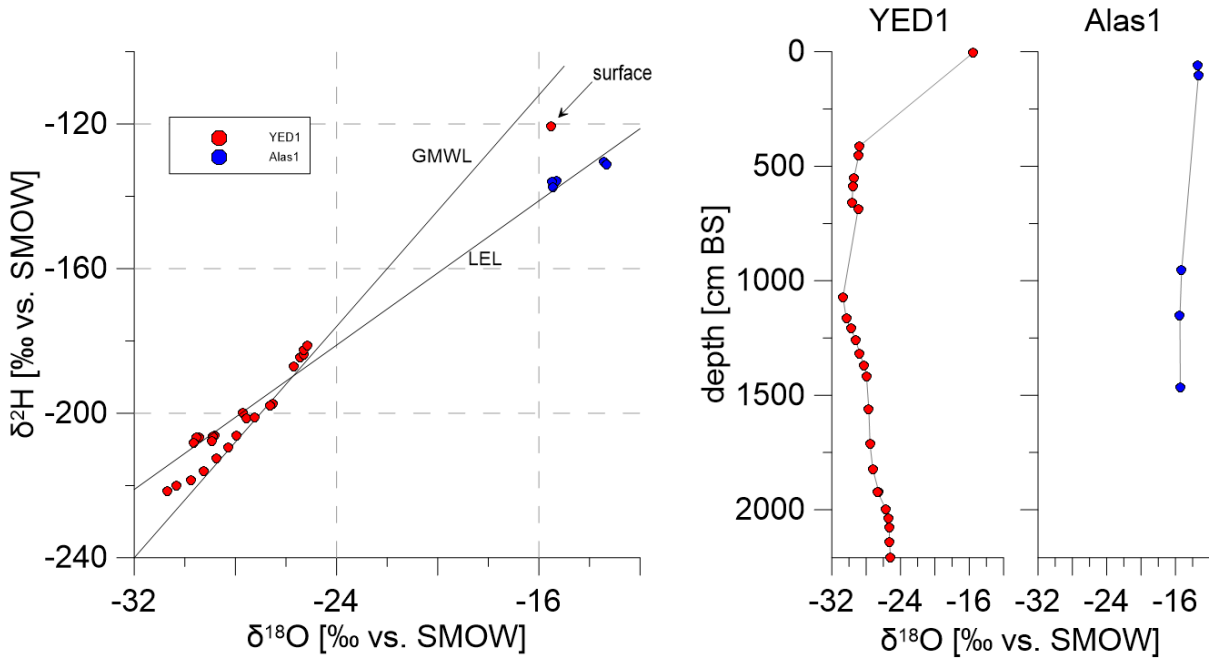

Figure 12 - left: Oxygen and hydrogen isotopes of YED1 and Alas1; GMWL: y= 8x; LEL of Central Yakutia (data until 2005); right: oxygen isotopes of YED1 and Alas1 plotted over depth, showing the sample locations within the cores

Stable water isotope data ($\delta^{18}O$ vs. $\delta^{2}H$) for both YED1 and Alas1 cores are plotted in **Figure 12** and the global meteoric water line (GMWL, slope = 8) is superimposed.

All YED1 samples (n= 23) (red, **Figure 12**) were taken from pore ice and roughly align with the GMWL showing $\delta^{18}O$ values between -25.16 ‰ vs. standard mean ocean water (SMOW) at 2209.5 cm BS and -30.7 ‰ vs. SMOW at 1071.5 cm BS. These values linearly increase from 1071.5 cm BS towards the bottom (2209.5 cm BS), whereas values between 413 and 658.5 cm BS decrease from -28.81 to -29.65 ‰ vs. SMOW. $\delta^{18}O$ value at 688 cm BS (-28.94 ‰ vs. SMOW) is slightly higher than above. One sample shows significantly higher values ($\delta^{18}O$= -15.53 ‰ vs. SMOW, $\delta^{2}H$= -120.76 ‰ vs. SMOW) but still aligns with the GMWL. For the other YED1 samples, $\delta^{2}H$ values range from -181.25 ‰ vs. SMOW (2209.5 cm BS) to -221.59 ‰ vs. SMOW (1071.5 cm BS) and show the same alignment as $\delta^{18}O$ values with a straight increase from 1071.5 to 2209.5 cm BS and from 413 cm BS (-206.29 ‰ vs. SMOW) down to 658.5 cm BS (-208.25 ‰ vs. SMOW) with 688 cm BS being an outlier with -207.65 ‰ vs. SMOW.

Alas1 water isotope samples (n= 5) (blue, **Figure 12**) are more off the GMWL and show generally higher $\delta^{18}O$ and $\delta^{2}H$ values rather similar to the YED1 surface sample. They align with the local evaporation line (LEL) of Central Yakutia and therefore represent precipitation or lake water (Wetterich et al., 2008). Two adjacent samples (61 cm BS and 103 cm BS) show very similar isotope values ($\delta^{18}O$= -13.44 ‰ vs. SMOW, $\delta^{2}H$= -130.37 ‰ vs. SMOW and $\delta^{18}O$= -13.33 ‰ vs. SMOW, $\delta^{2}H$= -131.3 ‰ vs. SMOW), while the remaining three samples (955, 1161 and 1464 cm BS) also show similar values for $\delta^{18}O$ (-15.28, -15.48 and -15.44 ‰ vs. SMOW) and for $\delta^{2}H$ (-135.85, -136.02 and -137.58 ‰ vs. SMOW). Again, the samples closer to the surface show higher $\delta^{18}O$ values (**Figure 12**).

The $\delta^{18}O$ values plotted against depth for both cores (**Figure 12**) identify the YED1 outlier from **figure 12** as the sample closest to the surface. They also identify the micro-clusters in Alas1 as adjacent samples.

4.4 Carbon ages

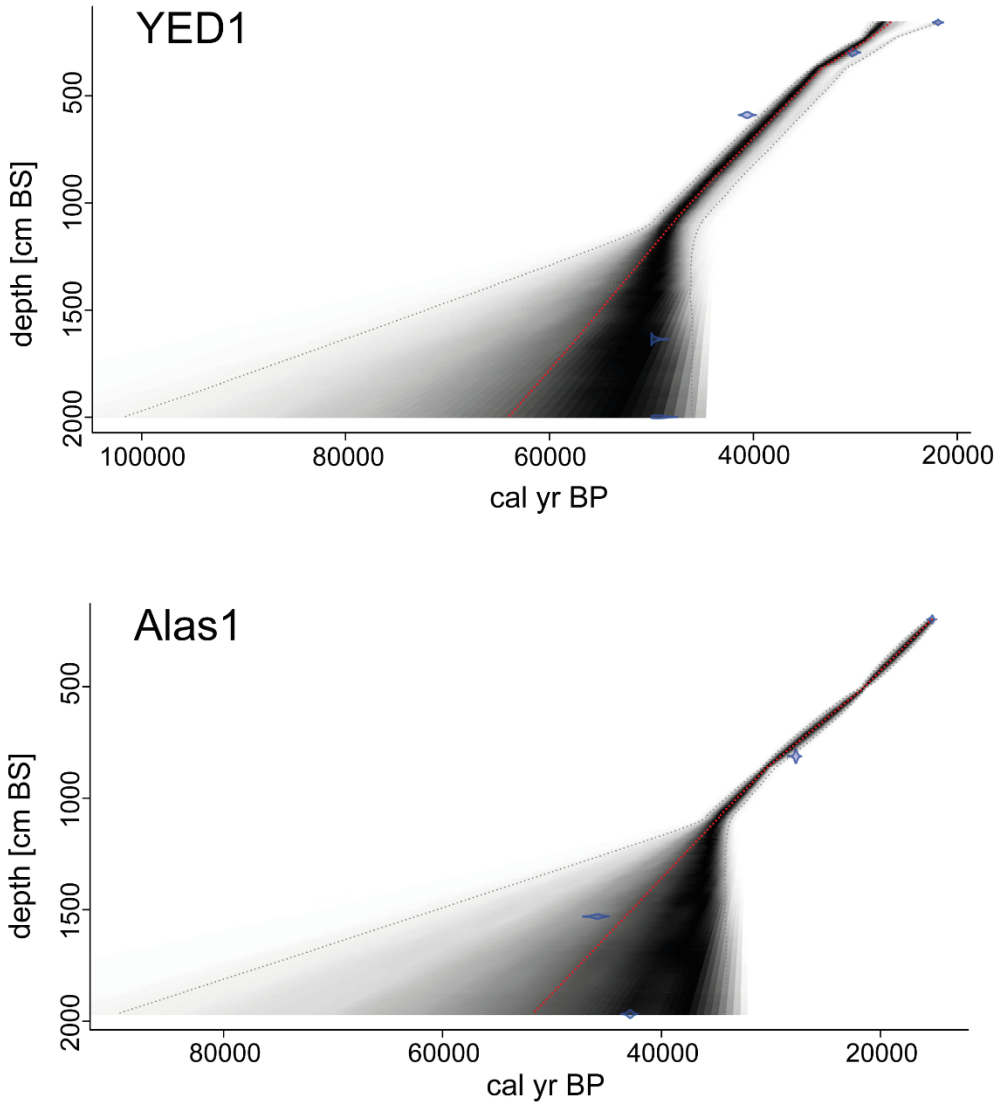

Figure 13 - Age-depth models for YED1 and Alas1; radiocarbon dating (Blaauw and Christen, 2011); dated samples are depicted in blue, shown including their uncertainties; median depicted in red; darker colour indicates higher model confidence

Calibrated ages (**Figures 9** and **10**) indicate an older age for YED1 (youngest sample at 21 890 cal yr BP; 157.5 cm BS) compared to Alas1 (15 287 cal yr BP; 199 cm BS). YED1 reaches the maximum measurable age of 49 000 yr BP (1636 cm BS) and therefore gives an infinite age for this sample. Below, a sample measured at 45 854 yr BP, calibrated to 49 232 cal yr BP (1998.5 cm BS) was found, while the oldest sample taken from Alas1 reaches an age of 45 870 cal yr BP (1530.5 cm BS) with a younger sample (42 865 cal yr BP; 1967.5 cm BS) below.

Age-depth modelling (**Figure 13**) shows high uncertainties in the lower parts of both cores. The areas of higher certainty (black, **Figure 13**) show a decrease in sedimentation rate over time towards more recent samples. In both models, certainty is good until approx. 1100 cm BS and spreads widely towards the bottom. Model medians give modelled bottom values of approx. 65 000 cal yr BP for YED1 and approx. 50 000 cal yr BP for Alas1, both contradicting the measured, younger ages.

All measured radiocarbon ages can be found in **table 5**.

4.5 Sedimentary characteristics

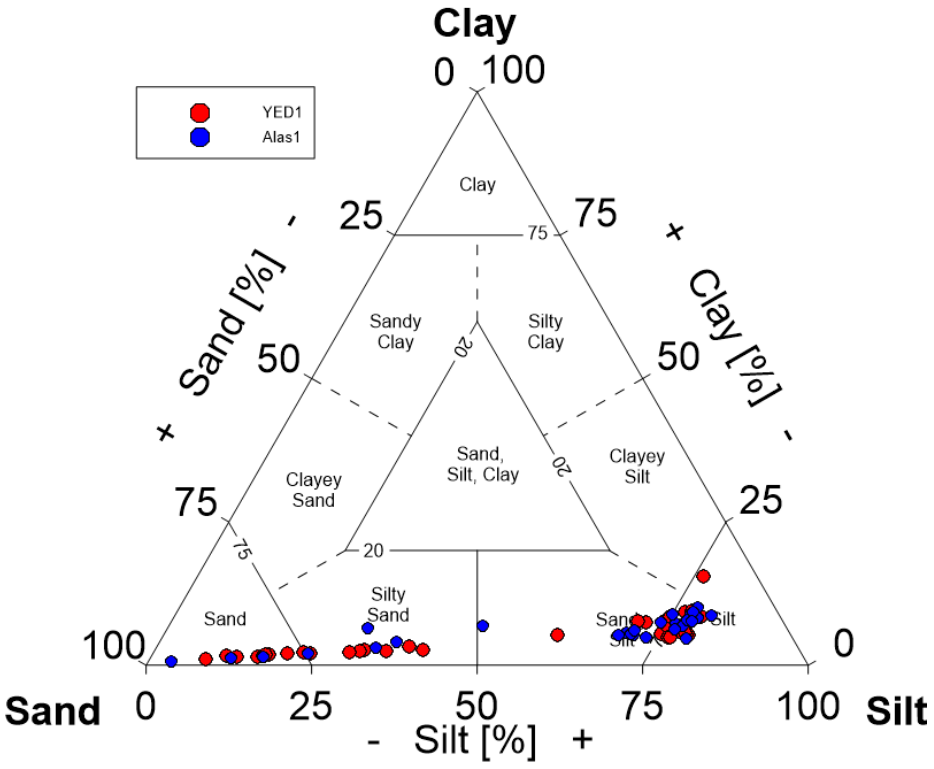

Figure 14 - Sediment triangle after Shepard for YED1 and Alas1 showing the grain size composition of each sample

As illustrated in **figure 14**, both YED1 (red, **Figure 14**) and Alas1 (blue, **Figure 14**) consists of two main grain size compositions. Both cores show a cluster at the border between silt and sandy silt at approx. 75 vol% silt and 20 vol% sand. The other grain size composition ranges between approx. 60 and 90 vol% sand with nearly no clay and silt ranging between 40 and 5 vol%. Both cores have an outlier or rather transition sample with 59.5 vol% silt and 35.2 vol% sand for YED1 (1007.5 cm BS) and 47.4 vol% silt and 45.8 vol% sand for Alas1 (395 cm BS).

The “high silt, low sand”-cluster for both cores consists of units 1 and 4 for each core which show a very similar material composition.

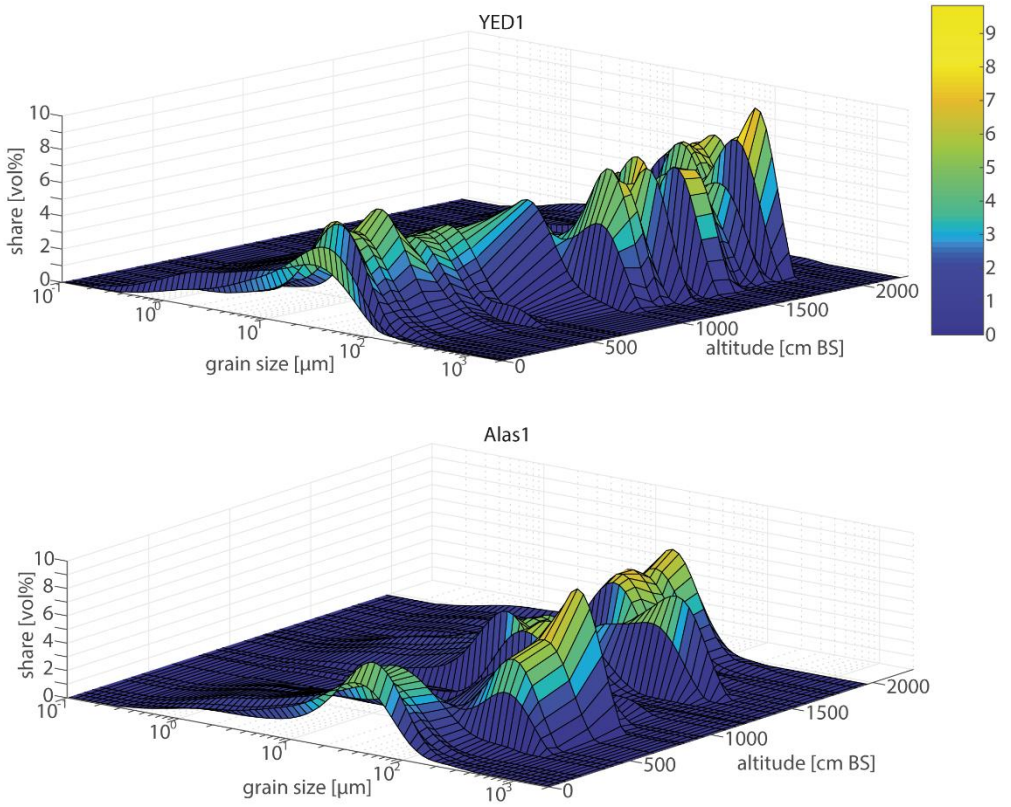

Figure 15 - 3D plots of grain size distribution within the YED1 and Alas1 cores over depth (created with MATLAB)

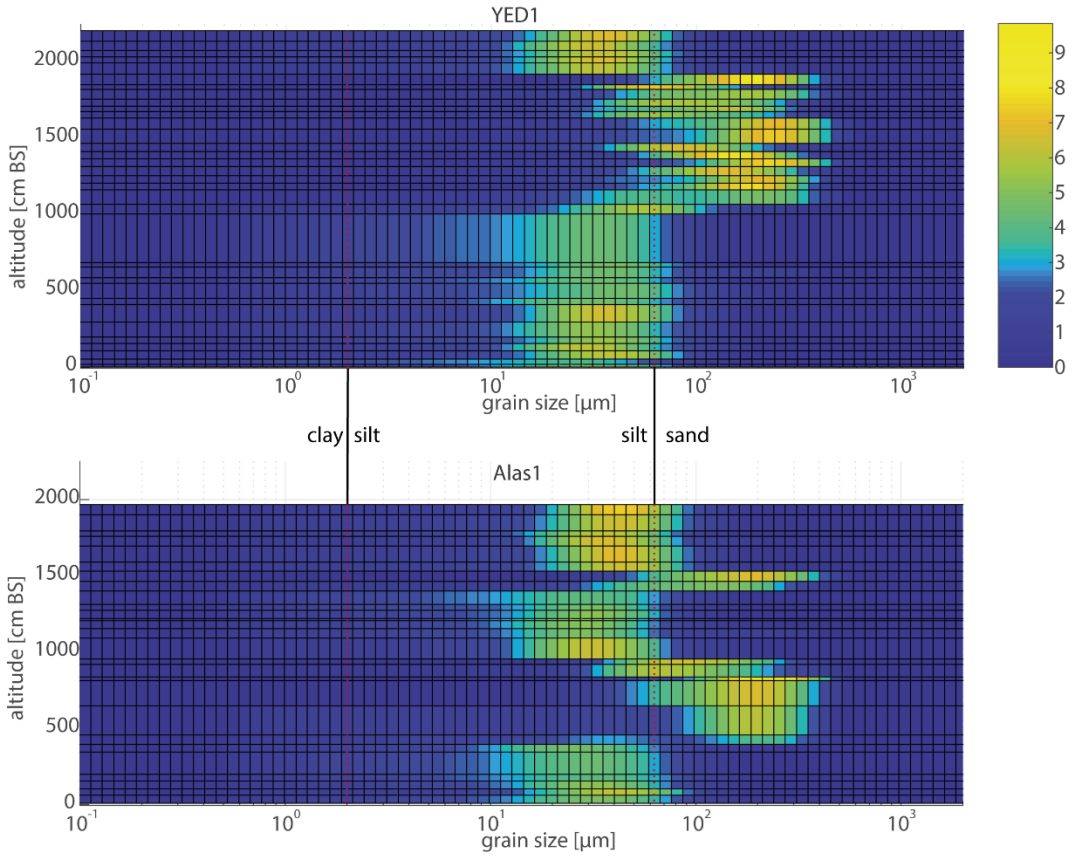

Figure 16 - Grain size distribution within YED1 and Alas1 cores over depth; top view of figure 16 (created with MATLAB)

Figures 15 and **16** both depict the grain size distribution in vol% over depth. Silty and less silty parts can be identified by both peak height (**Figure 15**) and colour (**Figures 15** and **16**; blue= low share, green= medium share, yellow= high share). Also, the shift towards sandier core parts can be seen by peak shifting towards the right (**Figure 15**) and the yellow area shifting towards the right (**Figure 16**).

The findings match those presented earlier in **figures 9** and **10**:

The YED1 core includes a sandy part between approx. 1000 and 1800 cm BS and returns to the previous grain size composition after the sandy intrusion.

Alas1 shows similar characteristics with a sandy part between 400 and 1000 cm BS and a steep sand peak approx. 1450 cm BS.

5 Discussion

5.1 Interpretation and context integration

The Alas1 core was drilled from the actual land surface within the alas basin which subsided during its unfrozen stages compared to the surrounding Yedoma. The Alas1 core is expected to consist of compacted and hydrologically and chemically reworked Yedoma deposits, overlain by lake sediments originating from the alas lake phases.

Radiocarbon ages show that the cores cover a timespan starting in the Late Pleistocene and covering the whole Holocene and reaching into the Pleistocene until approx. 12 000 cal yr BP. As for the existence of an active layer and vegetation cover, a recent age of the surface of the cores and Holocene ages for the whole undated uppermost 200 cm BS is assumed.

The age inversion (blue, **Figure 13**; **Table 5**) found in both cores in the lower third in measured radiocarbon ages is not represented in calibrated ages of YED1. This is simply due to excluding the infinite age measured at 1636 cm BS, σ= 0, which calibration software cannot work with. Also, the limit for calibration in Calib 7.1 is 50 000 cal yr BP which is reached in the lowest sample's maximum of YED1.

However, this age inversion implies several processes: The age inversion itself combined with the grain size peak, both found at approx. 45 000 cal yr BP in the Alas1 core, might represent a shift in external sediment input. In YED1 this inversion is found a little deeper at approx. 1700 cm BS and more than 49 000 cal yr BP, but the age-depth model (**Figure 13**) indicates that this inversion is still present at 45 000 cal yr BP. These two points in Alas1 and YED1 could therefore represent a change in sediment source around 45 000 cal yr BP. The sediment was probably altered in Alas1 by cryoturbation during the talik's refreezing or unfrozen lake conditions during active thermokarst processes.

The age distribution (**Figure 13**) in both cores shows a higher sedimentation rate at the core's bottom, slowing down towards the surface, especially from approx. 1500 cm BS to 1000 cm BS (Alas1) or 600 cm BS (YED1). This might indicate that during this phase from 45 000 to 35 000 cal yr BP the Alas1 was still a Yedoma permafrost, starting the alas development at the Pleistocene – Holocene boundary and corresponding warmer climate, as sedimentary processes should appear different within a lake. The detection limit of 49 000 cal yr BP for radiocarbon dating leads to high uncertainties for the YED1 age at approx. 1700 cm BS, as the measured sample could be slightly older or much older. This calibrated age being infinite results in the disappearance of the age inversion in **figure 9**.

As the sediment input varies, this can possibly be retraced by grain size distribution. Larger particles like sand are most often moved by fluvial processes, e. g. rivers or surface runoff from flooded areas. The transportation capacity of a river is mainly influenced by its water volume and velocity (Reineck

and Singh, 2012). This could mean that when rather coarse material was transported into the Yukechi Alas area, either the Lena River was flowing faster and flooded the area periodically, or the fine sediment material was transported by aeolian processes (Strauss et al., 2012). A reason for increased streaming velocity and more intense flooding could be precipitation changes or more rapid thawing and snow melt in springtime. If fine material was transported by aeolian processes, this indicates a change in wind systems. If it was deposited by fluvial processes, this indicates ponding surficial water, since fine material needs low streaming velocities to settle (Hjulström, 1939). Both scenarios require climatic variation at approx. 39 000 and 18 000 cal yr BP (**Figures 9** and **10**).

During 39 000 cal yr BP a shift to slightly higher insolation occurred in Eastern Siberia (Diekmann et al., 2017). This resulted in slightly colder summer but warmer winter temperatures. Evidence from lake Billyakh in Eastern Siberia show higher water levels (Diekmann et al., 2017), indicating a higher water availability which possibly resulted in higher sediment transportation capacities of rivers. An increase in flooding of former dry areas is likely to result from increased water availability in rivers. This could explain the increase in sand input into the Yukechi area.

The relevant climatic event at approx. 18 000 cal yr BP might have been the decline of the Last Glacial Maximum (Hubberten et al., 2004; Diekmann et al., 2017). The globally increasing availability of liquid water resulted in a global sea level rise of several meters (Lambeck and Chappell, 2001). This reduced the height differences between rivers' springs and mouths, resulting in decreasing vertical erosional power and reduction of streaming velocity (Hickin, 1995). In the consequence, the Yukechi area would have been flooded less often, resulting in less sand input.

However, the local setting of the study site on the very edge of the Abalakh terrace and the mean grain size (fine sand) of the sandy core units gives aeolian input from the area below the terrace and seasonal flooding input from the terrace's top as the most plausible source of the found fine sand, as this is found in adjacent areas as well (personal communication Christine Siegert). This scenario does not require a river at the study site which makes it more plausible, as the location on the terrace's edge and above the Lena river does not provide a sufficient water source for fluvial transport.

Fine material input in the studied cores would therefore originate from aeolian or occasional short-term flooding in YED1, while the ponding water of the alas lake would allow for low velocity depositions. In both fluvial scenarios, seasonal surface runoff and surface erosion are the most likely sources of fine sediment input.

The ice content increase with magnetic susceptibility decrease in Alas1 hints about a different type of sediment. This sediment must have been organic-poor already and lost its organic compounds more easily. It also has a lower magnetic susceptibility signal but a higher water holding capacity, resulting in higher ice content after refreezing. This is found in unit 2 of Alas1.

Magnetic susceptibility signals are also clearly linked to grain size distribution in both cores, showing that rather sandy sediments have higher magnetic susceptibility values while they tend to hold less to no carbon. This might be due to the larger pores found in sandy sediments, probably resulting in wash-out of organic compounds before freezing

This shows again that there have been shifts within the sedimentary regime that led to sedimentation of nearly organic-free sediments with a higher magnetic susceptibility. Units 1 and 4 (**Figures 9**, **10** and **14**) are very similar for most parameters, especially in grain size distribution. This indicates that after several shifts in sediment sources, the system shifted back to the former and probably original state.

5.2 Carbon accumulation and influencing factors

Carbon accumulation takes place during summer in unfrozen soil, when air temperatures allow for plant growth. These plants freeze during the following winter and become buried by sedimentation over consecutive years. This process, especially in syngenetic permafrost like that found in YED1, does not have to take place in situ, but anywhere in an adjacent sediment source area resulting in lateral transported organic-rich material. This lateral transport is often happening during springtime, when surface runoff erodes surficial sediments, transporting and re-depositing them fluvially (Battin et al., 2009).

Due to periodically unfrozen and/or lake covered conditions, moreover being a sediment trap due to geomorphologic position, it is very likely for the Alas1 core to hold more organic carbon in its uppermost lake sediment part compared to the Yedoma core (Walter Anthony et al., 2014). The mixture of unfrozen state and lake sediment input combined with epigenetic permafrost genesis enhance plant material input by sedimentation and in-situ growth as well as prevent this material from degradation by freezing quickly. This quick freezing is indicated by both isotope signals, matching liquid precipitation and ponding water (**Figure 12**) and larger non-layered cryostructures such as vertical bands (**Figure 7**). On the other hand, unfrozen conditions also allow for quicker degradation. This degradation can be estimated relatively by looking at the C/N ratios. A higher ratio represents a rather undecomposed or less decomposed state compared to lower ratios, indicating more strongly decomposed states of the organic matter (Kumada, 1987; Ping et al., 1998; Strauss et al., 2012). But in a Subarctic environment as Central Yakutia, this degradation is also limited to summer times. Therefore, the observed organic-poor areas cannot result only from degradation but a combination with much smaller input of organic material. This means that previously organic-poor material was transported into the area on which the lake formed later. Further decomposition the took place during lake cover and during sedimentation, giving TOC values below 0.1 vol% and C/N ratios close to zero.

The water isotopes found within Alas1 support this hypothesis as they imply lake water- or precipitation-saturated sediments that froze quickly without containing any winter precipitation signals. This can be seen as the Alas1 water isotope data are similar to the YED1 surface sample's isotope data (**Figure 12**).

In Alas1, expected portions of carbon having been fixed in situ during unfrozen, periodically lake-covered phases are expected, resulting in a mixture of plant species with a shift towards aquatic species compared to YED1 (**Figure 11**). YED1 also holds aquatic plant signals, which is probably due to fluvial surficial sediment transport.

A correlation between TOC values and absolute ice content is visible in YED1 as well as in Alas1 (**Figure 9** and **10**), as both values simultaneously rise and fall. This indicates permanently frozen and therefore stable conditions in affected depths, but also gives a hint on talik areas (YED1 100 – 200 cm BS, Alas1 100 – 800 cm BS). Downward water movement may have resulted higher ice contents at the talik's bottom.

There is a large part without TOC but with medium ice content found in YED1 (**Figure 9**, unit 3), correlating with a strong increase and generally higher values in magnetic susceptibility. The same correlation can be seen in Alas1 in units 2 and 3 and at 1400 cm BS, but with an increase in ice content from 800 to 1200 cm BS correlated with a decrease in magnetic susceptibility at the same depth (**Figure 10**, lower unit 2 and unit 3).

The combination of assumed fluvial sediment input with high streaming velocities for those core units with high sand content and very organic-poor sediment provides another scenario for the absence of TOC. During those phases with high flooding frequency and high streaming velocities, the water slowed

down enough to deposit the rather coarse, sandy sediment (Wilcock and Crowe, 2003). The fine organic material was kept suspended as velocity was still high enough for fine material transport and was therefore washed out of the area again.

In times with lower surface runoff velocities due to less available water and slower snow melt in springtime, probably combined with ponding water, the velocities were slow enough to deposit fine, organic-rich material.

If aeolian input is assumed, due to a lack of receiving waters found at the Abalakh terrace, a similar process might have caused the low TOC content. Small particles often provide insufficient surface area to be transported by wind, while large particles are often too heavy for aeolian sediment transport (Anderson et al., 1991). However, the found grain sizes in unit 3 are mainly fine sand and could therefore be just the right size for aeolian transportation.

The interpreted climatic changes at the beginning and end of the sandy units in YED1 and Alas1 might have caused changes in the regional wind regime as well, increasing wind velocities or changing wind direction. This might have caused the transport of more coarse material into the Yukechi area than before. The sediment would have likely been organic-poor as the coarse sandy material is deposited by slow wind, while fine organic matter is small enough for further aeolian sediment transport. Therefore, it is deposited at greater distance from the source area compared to sandy sediment (Pye, 1995).

The C/N values indicate at least a partial fluvial sediment input during the deposition of units 1 and 4 in both YED1 and Alas1 as both terrestrial and aquatic plant species were present (**Figure 11**).

Still, TOC contents are low, suggesting little vegetation cover, which favors deep permafrost formation. Vegetation works as an insulator in winter mainly because of its ability to trap snow.

The lack of carbon input from in situ-vegetation explains the total absence of TOC in times of external organic-poor sediment input.

5.3 Carbon losses and permafrost degradation

Due to talik conditions in both cores and especially the large talik found within the Alas1 core, the initial amount of carbon might have been reduced in both areas (Rivkina et al., 2000). But as carbon degradation still occurs below 0 °C, even if strongly slowed down, this could mean that carbon degradation did not only take place during talik conditions but also before, when the permafrost was already warmed up but still frozen.

Comparing **figures 9** and **10**, C/N ratios indicate similar composition states for the YED1 and Alas1 cores as C/N ratios all range around 8, if present, and are slightly lower in Alas1 from 1200 to 1400 cm BS, which represents a more decomposed state of organic matter. Since this point within Alas1 is overlain by organic-poor sediments and the organic-poor areas might represent lake phases. Organic matter decomposition rates are higher in lakes compared to frozen state (Conant et al., 2011) , while the lower C/N ratio between 1200 and 1400 cm BS might represent a drained and therefore dry and cold, but probably not permanently frozen state. The latter could allow for slightly higher decomposition than in permafrost state (C/N ratios ≥ 8 in **Figure 10**). The concurrent fall in ice content and rise in magnetic susceptibility are probably the result of a different sediment input between 1200 and 1400 cm BS in Alas1, supporting the drained lake phase hypothesis. As corresponding organic-poor areas are also found in YED1, lake cover cannot be the only reason for little organic content. On one hand, lake coverage does not result in complete degradation of organic matter but just more than in uncovered permafrost areas. On the other hand, YED1 was not covered by a lake within the last 50 000 cal yr BP.

This is contrary to the change in sedimentation rate indicating first lake stages after 35 000 cal yr BP. An explanation for this is model inaccuracy due to non-local but global modelling parameters (IntCal13) combined with cryoturbation during freezing and thawing events in early lake phases. It is more likely that lakes first formed in warmer climates at the beginning of the Holocene.

YED1 also shows a phase between 700 and 1900 cm BS (> 49 000 until 40 000 cal yr BP) with nearly no organic material and C/N values ~0 (**Figure 9**). Ice content, rising magnetic susceptibility, grain size distribution and the presence of an ice wedge (**Figure 9**) support the assumed change in sedimentation regime for this phase as lake cover of this original Yedoma was neither observed nor proved. As this whole core part is dated before the possible lake events in Alas1 and a similar sedimentation change but with lower susceptibility values is visible in Alas1, the idea of two alternating sedimentary regimes is strengthened.

When looking at the uppermost samples, ages of approx. 18 000 cal yr BP for YED1 and approx. 12 000 cal yr BP for Alas1 are shown by the model. As the next measured samples are located 155 cm (YED1, 21 890 cal yr BP) and 197 cm (Alas1, 15 287 cal yr BP), uncertainties include that surface samples could be more recent. However, this indicates very little sedimentation within the last 18 000 (approx. 150 cm) respectively 12 000 (approx. 200 cm) cal yr BP. On the other hand, it is more likely that permafrost has been degraded at the same rate sedimentation took place, probably removing last year's sediments during surficial spring flooding. The remaining 150 cm in YED1 and 200 cm in Alas1 are part of the summer's active layer and are likely to hold recent organic material. This would result in either recent carbon ages or mixed and partially reversed carbon ages due to cryoturbation within the active layer during thawing in summer and refreezing in winter.

No ice wedge, a typical feature of Yedoma deposits (Strauss et al., 2017), was found in Alas1. This is explained by the unfrozen state during lake coverage, which is retraceable by the existence of a still large talik. It is very likely that ice wedges existed within the former Yedoma deposits and thawed out during alas development. This thawing often results in surface subsidence, leaving the newly TOC vulnerable to degradation, while the melt water itself also supports TOC degradation (Vonk et al., 2013a).

5.4 Pathway of local carbon pools

There are many similarities found between YED1 and Alas1 core; all differences such as ice content, grain size distribution (**Figures 9** and **10**), carbon ages and sedimentation rates (**Figure 13**) can be retraced to either variation between slightly different locations and/or lake coverage. Especially the lake influence could provide implications for future Yedoma state as in a warming climate, an increase in the number and size of lakes has already been observed in the continuous permafrost zone (Smith et al., 2005) but in particular in Central Yakutia (Nitze et al., 2017). This would lead to larger Yedoma areas being flooded, thawed and eventually refrozen, resulting in characteristics similar to Alas1.

As lake coverage would also increase the decomposition of organic carbon currently stored in Yedoma, this would mean an increase of atmospheric carbon by carbon release from former Yedoma deposits which are vulnerable to climate warming due to their high ice contents (Schneider von Deimling et al., 2015). Despite having less carbon compared to other Yedoma deposits (compared to overall mean of 42.9 kg/m³ carbon (Strauss et al., 2013, 2017), the 5.9 kg/m³ carbon (average of YED1) are one part of the potentially reactivated carbon pool. Yedoma deposits also cover large portions of Arctic ground surface (Strauss et al., 2012) and they are vulnerable to thawing and subsidence. This vulnerability is partially triggered by more, thicker snow cover isolating against cold winter temperatures.

Furthermore, the ice wedges in Yedoma deposits will thaw in a future warming climate, starting a mechanism of self-sustaining decomposition (Khvorostyanov et al., 2008; Vonk et al., 2013b), in which

low phenolic contents in ice wedge meltwater enhance TOC degradation. This process produces heat which enhances further thawing, enhancing further decomposition (Vonk et al., 2013b).

Figure 14 supports the hypothesis that both YED1 and Alas1 consist of material originating from the same sources, allowing for the assumption that both deposits have been formed by the same processes. Alteration of the alas therefore happened with a minimal accumulation rate after formation. In addition to thermokarst processes, external factors such as sediment input from external and changing areas or processes influenced both deposits.

It is therefore possible that the found sand was accumulated in the location of YED1 and was then transported to the Alas1 site before or during lake formation.

6 Conclusion

The permafrost characteristics found in the Alas1 core show a pre-lake state very similar to the YED1 core material. Carbon characteristics and distribution differ due to changed accumulation and decomposition conditions as well as ground subsidence during unfrozen conditions.

The main processes for carbon storage in the Yukechi area are syngenetic permafrost accumulation, thermokarst lake development and varying material input. The syngenetic Yedoma deposits found in this area show very little disturbances and a highly preserved state in terms of carbon content. The material taken from the Yukechi Alas site shows characteristics that are typical for lake-covered permafrost deposits, such as talik formation and higher amounts of carbon compared to the adjacent Yedoma. Adding to this, the varying material input during the late Pleistocene previously lead to smaller carbon content than throughout the other core units.

The amount of organic carbon expected to be stored in Yedoma permafrost (Zimov et al., 2006; Strauss et al., 2012) is not supported by these findings as carbon content is low in the YED1 core. This might either be due to a local exception in material origin or an exceptional high decomposition rate of organic matter during deposition. Therefore, the thawing of permafrost in this region might have less climatic impact than previously thought (Strauss et al., 2017), in terms of carbon release in the context of climate change. Especially between 1200 and 1900 cm BS only small amounts of carbon are contained. But as also high ice contents were found in the Yukechi area, including an ice wedge in YED1, further global warming might efficiently thaw the Central Yakutian permafrost and release the stored carbon.

In aspect of their high vulnerability shown by the origin and pathway of Yedoma-stored organic carbon (Vonk et al., 2013a), those Yedoma deposits with high carbon content could have a high impact on the arctic amplification in terms of global climate change (Serreze and Barry, 2011). The high ice contents found in these deposits supply high potential for further ground subsidence related to climate warming in both Yedoma and alas deposits. This will put human infrastructure to further stress (Nelson et al., 2002).

To determine whether fluvial or aeolian transport have been the main sediment input pathways during 39 000 and 18 000 cal yr BP, a closer look on mineral composition and grain shapes of the deposited material has to be taken.

7 References

Anderson, R.S., Sørensen, M., Willetts, B.B., 1991. A review of recent progress in our understanding of aeolian sediment transport. Aeolian Grain Transp. 1, Acta Mechanica Supplementum 1–19. https://doi.org/10.1007/978-3-7091-6706-9_1

Bartsch, A., Seifert, F.M., 2012. The ESA DUE Permafrost project - A service for high latitude research, Geoscience and Remote Sensing Symposium (IGARSS). IEEE International.

Battin, T.J., Luyssaert, S., Kaplan, L.A., Aufdenkampe, A.K., Richter, A., Tranvik, L.J., 2009. The boundless carbon cycle. Nat. Geosci. 2, 598–600.

Blaauw, M., Christen, J.A., 2011. Flexible paleoclimate age-depth models using an autoregressive gamma process. Bayesian Anal. 6, 457–474. https://doi.org/10.1214/11-BA618

Blott, S.J., Pye, K., 2001. GRADISTAT. Kenneth Pye Associates Ltd., England.

Brown, J., Ferrians Jr, O.J., Heginbottom, J.A., Melnikov, E.S., 2002. | National Snow and Ice Data Center [WWW Document]. Circum-Arct. Map Permafr. Ground-Ice Cond. Version 2. URL https://nsidc.org/data/ggd318 (accessed 11.10.17).

Brown, J., Ferrians Jr, O.J., Heginbottom, J.A., Melnikov, E.S., 1997. Circum-Arctic map of permafrost and ground-ice conditions. US Geological Survey Reston, VA.

Butler, R.F., 1992. Paleomagnetism: magnetic domains to geologic terranes. Blackwell Scientific Publications Boston.

Conant, R.T., Ryan, M.G., Ågren, G.I., Birge, H.E., Davidson, E.A., Eliasson, P.E., Evans, S.E., Frey, S.D., Giardina, C.P., Hopkins, F.M., Hyvönen, R., Kirschbaum, M.U.F., Lavallee, J.M., Leifeld, J., Parton, W.J., Steinweg, J.M., Wallenstein, M.D., Wetterstedt, J.Å.M., Bradford, M.A., 2011. Temperature and soil organic matter decomposition rates – synthesis of current knowledge and a way forward. Glob. Change Biol. 17, 3392–3404. https://doi.org/10.1111/j.1365-2486.2011.02496.x

Coplen, T.B., Brand, W.A., Gehre, M., Gröning, M., Meijer, H.A.J., Toman, B., Verkouteren, R.M., 2006. New Guidelines for δ13C Measurements. Anal. Chem. 78, 2439–2441. https://doi.org/10.1021/ac052027c

Dearing, J., 1999. Magnetic susceptibility. Environ. Magn. Pract. Guide 6, 35–62.

Desyatkin, A.R., Takakai, F., Hatano, R., 2014. Flood effect on CH4 emission from the alas in Central Yakutia, East Siberia. Soil Sci. Plant Nutr. 60, 242–253. https://doi.org/10.1080/00380768.2014.883486

Diekmann, B., Pestryakova, L., Nazarova, L., Subetto, D., Tarasov, P.E., Stauch, G., Thiemann, A., Lehmkuhl, F., Biskaborn, B., Kuhn, G., Henning, D., Müller, S., 2017. Late Quarternary Lake Dynamics in the Verkhoyansk Mountains of Eastern Siberia: Implications for Climate and Glaciation History. Polarforschung 86, 97–110.

Fedorov, A.N., 2006. Present post-disturbance dynamics of permafrost in Central Yakutia, in: Hatano, R.; Guggenberger, G.: Symptom of Environmental Change in Siberian Permafrost Region. Hokkaido University Press, Sapporo.

Fedorov, A.N., Konstantinov, P., 2003. Observations of surface dynamics with thermokarst initiation, Yukechi site, Central Yakutia, in: Phillips, M. ; Springman, S.M. ; Arenson, L.U. : Permafrost - Proceedings of the 8th International Conference on Permafrost. University of Zurich, Zürich, Switzerland.

Fedorov, A.N., Konstantinov, P.Y., Vassiliev, I.S., Bosikov, N.P., Torgovkin, Y.I., Samsonova, V.V., 1998. Observations of permafrost-landscape dynamics related to anthropogenic disturbances, Yukechi study site, Central Yakutia. Permafr. Proc. Seventh Int. Conf. 259–263.

Ferrians, O.J., Kachadoorian, R., Greene, G.W., 1969. Permafrost and related engineering problems in Alaska. US Government Printing Office.

French, H.M., 2007. The Periglacial Environment, 3rd edition. ed. Wiley.

Heginbottom, J.A., Brown, J., Humlum, O., Svensson, H., 2012. Permafrost and Periglacial Environments. US Geol. Surv. Prof. Pap.

Hickin, E.J. (Ed.), 1995. River Geomorphology, 1 edition. ed. Wiley, Chichester.

Hjulström, F., 1939. Recent Marine Sediments—a Symposium.

Horita, J., Ueda, A., Mizukami, K., Takatori, I., 1989. Automatic δD and δ18O analyses of multi-water samples using H2- and CO2-water equilibration methods with a common equilibration set-up. Int. J. Rad. Appl. Instrum. [A] 40, 801–805. https://doi.org/10.1016/0883-2889(89)90100-7

Hubberten, H.W., Andreev, A., Astakhov, V.I., Demidov, I., Dowdeswell, J.A., Henriksen, M., Hjort, C., Houmark-Nielsen, M., Jakobsson, M., Kuzmina, S., Larsen, E., Lunkka, J.P., Lyså, A., Mangerud, J., Möller, P., Saarnisto, M., Schirrmeister, L., Sher, A.V., Siegert, C., Siegert, M.J., Svendsen, J.I., 2004. The periglacial climate and environment in northern Eurasia during the Last Glaciation. Quat. Sci. Rev., Quaternary Environments of the Eurasian North (QUEEN) 23, 1333–1357. https://doi.org/10.1016/j.quascirev.2003.12.012

Hugelius, G., Strauss, J., Zubrzycki, S., Harden, J.W., Schuur, E. a. G., Ping, C.-L., Schirrmeister, L., Grosse, G., Michaelson, G.J., Koven, C.D., O'Donnell, J.A., Elberling, B., Mishra, U., Camill, P., Yu, Z., Palmtag, J., Kuhry, P., 2014. Estimated stocks of circumpolar permafrost carbon with quantified uncertainty ranges and identified data gaps. Biogeosciences Online 11. https://doi.org/10.5194/bg-11-6573-2014

Hunt, R., 1982. Plant growth curves. The functional approach to plant growth analysis. Edward Arnold Ltd., London, UK.

ISO, EN, 2017. ISO 14688-1: 2017: Geotechnical investigation and testing - Identification and classification of soil - Part 1: Identification and description.

Jongejans, L.L., Strauss, J., Lenz, J., Peterse, F., Mangelsdorf, K., Fuchs, M., Grosse, G., 2018. Organic carbon characteristics in yedoma and thermokarst deposits on Baldwin Peninsula, Wet-Alaska. Biogeosciences Discuss. 29. https://doi.org/doi.org/10.5194/bg-2018-151

Katamura, F., Fukuda, M., Bosikov, N.P., Desyatkin, R.V., Nakamura, T., Moriizumi, J., 2006. Thermokarst Formation and Vegetation Dynamics Inferred from A Palynological Study in Central Yakutia, Eastern Siberia, Russia. Arct. Antarct. Alp. Res. 38, 561–570. https://doi.org/10.1657/1523-0430(2006)38[561:TFAVDI]2.0.CO;2

Khvorostyanov, D.V., Krinner, G., Ciais, P., Heimann, M., Zimov, S.A., 2008. Vulnerability of permafrost carbon to global warming. Part I: model description and role of heat generated by organic matter decomposition. Tellus B 60, 250–264. https://doi.org/10.1111/j.1600-0889.2007.00333.x

Köppen, W., Geiger, R., 1930. Handbuch der Klimatologie. Gebrüder Borntraeger Berlin, Germany.

Kumada, K., 1987. Chemistry of soil organic matter. Dev. Soil Sci.

Lambeck, K., Chappell, J., 2001. Sea Level Change Through the Last Glacial Cycle. Science 292, 679–686. https://doi.org/10.1126/science.1059549

Meyer, H., Schönicke, L., Wand, U., Hubberten, H.-W., Friedrichsen, H., 2000. Isotope studies of hydrogen and oxygen in ground ice-experiences with the equilibration technique. Isotopes Environ. Health Stud. 133–149.

Meyers, P.A., 1997. Organic geochemical proxies of paleoceanographic, paleolimnologic, and paleoclimatic processes. Org Geochem 213–250.

Nazarova, L., Lüpfert, H., Subetto, D., Pestryakova, L., Diekmann, B., 2013. Holocene climate conditions in central Yakutia (Eastern Siberia) inferred from sediment composition and fossil chironomids of Lake Temje. Quat. Int., The Baikal-Hokkaido Archaeology Project: Environmental archives, proxies and reconstruction approaches 290–291, 264–274. https://doi.org/10.1016/j.quaint.2012.11.006

Nelson, F.E., Anisimov, O.A., Shiklomanov, N.I., 2002. Climate Change and Hazard Zonation in the Circum-Arctic Permafrost Regions. Nat. Hazards 26, 203–225. https://doi.org/10.1023/A:1015612918401

Nitze, I., Grosse, G., Jones, B.M., Arp, C.D., Ulrich, M., Fedorov, A., Veremeeva, A., 2017. Landsat-Based Trend Analysis of Lake Dynamics across Northern Permafrost Regions. Remote Sens. 9, 640. https://doi.org/10.3390/rs9070640

Ping, C.L., Bockheim, J.G., Kimble, J.M., Michaelson, G.J., Walker, D.A., 1998. Characteristics of cryogenic soils along a latitudinal transect in arctic Alaska. J. Geophys. Res. Atmospheres 103, 28917–28928. https://doi.org/10.1029/98JD02024

Pye, K., 1995. The nature, origin and accumulation of loess. Quat. Sci. Rev., Aeolian Sediments in the Quaternary Record 14, 653–667. https://doi.org/10.1016/0277-3791(95)00047-X

R Core Team, 2016. R: A language and environment for statistical computing. R Foundation for Statistical Computing, Vienna, Austria.

Reimer, P.J., Bard, E., Bayliss, A., Beck, J.W., Blackwell, P.G., Ramsey, C.B., Buck, C.E., Cheng, H., Edwards, R.L., Friedrich, M., Grootes, P.M., Guilderson, T.P., Haflidason, H., Hajdas, I., Hatté, C., Heaton, T.J., Hoffmann, D.L., Hogg, A.G., Hughen, K.A., Kaiser, K.F., Kromer, B., Manning, S.W., Niu, M., Reimer, R.W., Richards, D.A., Scott, E.M., Southon, J.R., Staff, R.A., Turney, C.S.M., Plicht, J. van der, 2013. IntCal13 and Marine13 Radiocarbon Age Calibration Curves 0–50,000 Years cal BP. Radiocarbon 55, 1869–1887. https://doi.org/10.2458/azu_js_rc.55.16947

Reineck, H.-E., Singh, I.B., 2012. Depositional Sedimentary Environments: With Reference to Terrigenous Clastics. Springer Science & Business Media.

Rivkina, E.M., Friedmann, E.I., McKay, C.P., Gilichinsky, D.A., 2000. Metabolic Activity of Permafrost Bacteria below the Freezing Point. Appl. Environ. Microbiol. 66, 3230–3233. https://doi.org/10.1128/AEM.66.8.3230-3233.2000

Skålin, Norwegian Meteorological Institute, 2018. Climate data for Yakutsk, Sakha (Russia).

Schirrmeister, L., Froese, D., Tumskoy, V., Grosse, G., Wetterich, S., 2013. Yedoma: Late Pleistocene ice-rich syngenetic permafrost of Beringia, in: Encyclopedia of Quaternary Science. 2nd Edition. Elsevier, pp. 542–552.

Schneider von Deimling, T., Grosse, G., Strauss, J., Schirrmeister, L., Morgenstern, A., Schaphoff, S., Meinshausen, M., Boike, J., 2015. Observation-based modelling of permafrost carbon fluxes with accounting for deep carbon deposits and thermokarst activity. Biogeosciences 12, 3469–3488. https://doi.org/Schneider von Deimling, T. , Grosse, G. , Strauss, J. , Schirrmeister, L. , Morgenstern, A. , Schaphoff, S. , Meinshausen, M. and Boike, J. (2015) Observation-based modelling of permafrost carbon fluxes with accounting for deep carbon deposits and thermokarst activity , Biogeosciences, 12 (11), pp. 3469-3488 . doi:10.5194/bg-12-3469-2015 <http://doi.org/10.5194/bg-12-3469-2015> , hdl:10013/epic.45687

Schuur, E.A.G., Bockheim, J., Canadell, J.G., Euskirchen, E., Field, C.B., Goryachkin, S.V., Hagemann, S., Kuhry, P., Lafleur, P.M., Lee, H., Mazhitova, G., Nelson, F.E., Rinke, A., Romanovsky, V.E., Shiklomanov, N., Tarnocai, C., Venevsky, S., Vogel, J.G., Zimov, S.A., 2008. Vulnerability of Permafrost Carbon to Climate Change: Implications for the Global Carbon Cycle. BioScience 58, 701–714. https://doi.org/10.1641/B580807

Serreze, M.C., Barry, R.G., 2011. Processes and impacts of Arctic amplification: A research synthesis. Glob. Planet. Change 77, 85–96. https://doi.org/10.1016/j.gloplacha.2011.03.004

Smith, L.C., Sheng, Y., MacDonald, G.M., Hinzman, L.D., 2005. Disappearing Arctic Lakes. Science, New Series 308, 1429.

Strauss, J., Schirrmeister, L., Grosse, G., Fortier, D., Hugelius, G., Knoblauch, C., Romanovsky, V., Schädel, C., Schneider von Deimling, T., Schuur, E.A.G., Shmelev, D., Veremeeva, A., 2017. Deep Yedoma permafrost: A synthesis of depositional characteristics and carbon vulnerability. Earth-Sci. Rev. 75–86. https://doi.org/10.1016

Strauss, J., Schirrmeister, L., Grosse, G., Wetterich, S., Ulrich, M., Herzschuh, U., Hubberten, H.-W., 2013. The deep permafrost carbon pool of the Yedoma region in Siberia and Alaska. Geophys. Res. Lett. 40, 6165–6170. https://doi.org/10.1002/2013GL058088

Strauss, J., Schirrmeister, L., Mangelsdorf, K., Eichhorn, L., Wetterich, S., Herzschuh, U., 2015. Organic-matter quality of deep permafrost carbon – a study from Arctic Siberia. Biogeosciences 12, 2227–2245. https://doi.org/10.5194/bg-12-2227-2015

Strauss, J., Schirrmeister, L., Wetterich, S., Borchers, A., Davydov, S.P., 2012. Grain-size properties and organic-carbon stock of Yedoma Ice Complex permafrost from the Kolyma lowland, northeastern Siberia. Glob. Biogeochem. Cycles 26. https://doi.org/10.1029/2011GB004104

Stuiver, M., Reimer, P.J., Reimer, R.W., 2018. CALIB 7.1 [WWW program].

Troeva, E.I., Isaev, A.P., Cherosov, M.M., Karpov, N.S., 2010. The Far North:: Plant Biodiversity and Ecology of Yakutia. Springer Science & Business Media.

Ulrich, M., Wetterich, S., Rudaya, N., Frolova, L., Schmidt, J., Siegert, C., Fedorov, A.N., Zielhofer, C., 2017. Rapid thermokarst evolution during the mid-Holocene in Central Yakutia, Russia. The Holocene 27, 1899–1913. https://doi.org/10.1177/0959683617708454

van Everdingen, R., 2005. Multi-language glossary of permafrost and related ground-ice terms. National Snow and Ice Data Center/World Data Center for Glaciology, Boulder, CO. World Wide Web Address Httpnsidc Orgfgdcglossary 63–64.

Vonk, J.E., Mann, P.J., Davydov, S., Davydova, A., Spencer, R.G., Schade, J., Sobczak, W.V., Zimov, N., Zimov, S., Bulygina, E., Eglinton, T.I., Holmes, R.M., 2013a. High biolability of ancient permafrost carbon upon thaw. Geophys. Res. Lett. 40, 2689–2693. https://doi.org/10.1002/grl.50348

Vonk, J.E., Mann, P.J., Dowdy, K.L., Davydova, A., Davydov, S.P., Zimov, N., Spencer, R.G.M., Bulygina, E.B., Eglinton, T.I., Holmes, R.M., 2013b. Dissolved organic carbon loss from Yedoma permafrost amplified by ice wedge thaw. Environ. Res. Lett. 8, 035023. https://doi.org/10.1088/1748-9326/8/3/035023

Walter Anthony, K.M., Zimov, S.A., Grosse, G., Jones, M.C., Anthony, P.M., Iii, F.S.C., Finlay, J.C., Mack, M.C., Davydov, S., Frenzel, P., Frolking, S., 2014. A shift of thermokarst lakes from carbon sources to sinks during the Holocene epoch. Nature 511, 452. https://doi.org/10.1038/nature13560

Weiss, N., Blok, D., Elberling, B., Hugelius, G., Jørgensen, C.J., Siewert, M.B., Kuhry, P., 2016. Thermokarst dynamics and soil organic matter characteristics controlling initial carbon release from permafrost soils in the Siberian Yedoma region. Sediment. Geol., Limnological processes in permafrost environments 340, 38–48. https://doi.org/10.1016/j.sedgeo.2015.12.004

Wetterich, S., Herzschuh, U., Meyer, H., Pestryakova, L., Plessen, B., Lopez, C.M.L., Schirrmeister, L., 2008. Evaporation effects as reflected in freshwater and ostracod calcite from modern environments in Central and Northeast Yakutia (East SIberia, Russia). Hydrobiologia 171–195. https://doi.org/10.1007/s10750-008-9505-y

Wilcock, P.R., Crowe, J.C., 2003. Surface-based Transport Model for Mixed-Size Sediment. J. Hydraul. Eng. 129, 120–128. https://doi.org/10.1061/(ASCE)0733-9429(2003)129:2(120)

Zhang, T., Barry, R.G., Knowles, K., Heginbottom, J.A., Brown, J., 1999. Statistics and characteristics of permafrost and ground-ice distribution in the Northern Hemisphere. Polar Geogr. 23, 132–154. https://doi.org/10.1080/10889379909377670

Zimov, S.A., Davydov, S.P., Zimova, G.M., Davydova, A.I., Schuur, E.A.G., Dutta, K., Chapin, F.S., 2006. Permafrost carbon: Stock and decomposability of a globally significant carbon pool. Geophys. Res. Lett. 33. https://doi.org/10.1029/2006GL027484

Appendix

Tables

Table 1 - YED1 - sedimentary data

Sample	depth [cm BS]	absolut ice content [wt%]	magnetic susceptibility (low frequency) [10^{-8} m^3 kg^{-1}]	clay [vol%]	silt [vol%]	sand [vol%]	bulk density [g/cm^3]
YUK15-YED1 0 - 8 cm	4	24.50	15.358	5.7	78.8	15.5	1.36
YUK15-YED1 19 - 23 cm	21	20.00	52.601	15.5	76.5	8.1	-
YUK15-YED1 54 - 57 cm	55.5	25.62	98.984	6.2	75.5	18.3	1.33
YUK15-YED1 108 - 112 cm	110	14.58	82.989	5.7	78.0	16.3	-
YUK15-YED1 155 - 160 cm	157.5	20.99	90.395	7.7	74.5	17.8	1.50
YUK15-YED1 198 - 202 cm	200	19.69	73.505	6.9	77.4	15.6	-
YUK15-YED1 295 - 301 cm	298	29.39	118.630	5.4	75.0	19.6	1.20
YUK15-YED1 409 - 417 cm	413	34.77	94.634	6.9	75.1	18.0	1.04
YUK15-YED1 450 - 457 cm	453.5	35.63	102.035	7.5	71.7	20.8	1.02
YUK15-YED1 548 - 557 cm	552.5	40.76	95.898	9.2	76.9	14.0	0.88
YUK15-YED1 586 - 593 cm	589.5	30.73	92.446	7.6	70.5	21.8	1.16
YUK15-YED1 655 - 662 cm	658.5	30.94	100.295	8.4	74.9	16.7	1.15
YUK15-YED1 685 - 691 cm	688	57.40	108.118	9.5	77.6	12.8	0.54
YUK15-YED1 1005 - 1010 cm	1007.5	53.68	177.455	5.3	59.5	35.2	0.61
YUK15-YED1 1069 - 1074 cm	1071.5	32.12	120.468	2.5	35.1	62.4	1.12
YUK15-YED1 1163 - 1167 cm	1165	23.67	155.112	1.4	16.2	82.4	1.40
YUK15-YED1 1206 - 1212 cm	1209	24.68	197.751	2.1	23.7	74.1	1.36
YUK15-YED1 1256 - 1259 cm	1257.5	26.80	216.721	2.0	20.4	77.5	1.28
YUK15-YED1 1315 - 1322 cm	1318.5	21.69	139.786	1.7	16.9	81.4	1.49
YUK15-YED1 1364 - 1374 cm	1369	24.31	258.837	1.4	13.0	85.6	1.37
YUK15-YED1 1414 - 1419 cm	1416.5	27.61	223.246	2.6	31.6	65.8	1.26
YUK15-YED1 1467 - 1472 cm	1469.5	15.82	155.078	1.8	17.6	80.6	-
YUK15-YED1 1560 - 1566 cm	1563	18.99	233.939	1.8	17.2	81.1	-
YUK15-YED1 1632 - 1640 cm	1636	20.40	211.483	3.2	38.2	58.6	1.52
YUK15-YED1 1677 - 1681 cm	1679	19.75	285.023	2.4	31.1	66.5	-
YUK15-YED1 1711 - 1717 cm	1714	19.06	213.984	2.3	29.5	68.2	-
YUK15-YED1 1758 - 1762 cm	1760	16.53	240.126	2.2	22.6	75.2	-
YUK15-YED1 1820 - 1828 cm	1824	26.84	183.424	2.7	40.4	56.9	1.28
YUK15-YED1 1853 - 1858 cm	1855.5	15.51	256.195	1.1	8.5	90.3	-
YUK15-YED1 1920 - 1927 cm - A (sand)	1923.5	22.28	207.877	1.6	11.4	87.0	1.45
YUK15-YED1 1920 - 1927 cm - B	1923.5	36.29	155.359	4.8	76.4	18.8	1.00
YUK15-YED1 1996 - 2001 cm	1998.5	53.59	123.684	5.2	79.4	15.4	0.61
YUK15-YED1 2033 - 2039 cm	2036	35.22	126.050	4.8	76.7	18.5	1.03
YUK15-YED1 2076 - 2081 cm	2078.5	46.77	153.183	5.3	79.0	15.7	0.75
YUK15-YED1 2135 - 2145 cm	2140	30.71	95.060	5.7	78.6	15.7	1.16
YUK15-YED1 2207 - 2212 cm	2209.5	35.82	60.726	8.5	79.6	12.0	1.01

Table 2 - YED1 - chemical data

Sample	TC [wt%]	TN [wt%]	TOC [wt%]	TOC/CN ratio	TOC [kg/m³]	δ2D [‰ vs. SMOW]	δ18O [‰ vs. SMOW]	δ13C [‰VPDB]
YUK15-YED1 0 - 8 cm	1.248	<0.100	<0.100	-	1.36	-120.76	-15.53	-
YUK15-YED1 19 - 23 cm	1.776	<0.100	1.250	12.497	-	-	-	-28.07
YUK15-YED1 54 - 57 cm	0.984	<0.100	<0.100	-	1.32	-	-	-
YUK15-YED1 108 - 112 cm	1.312	<0.100	<0.100	-	-	-	-	-
YUK15-YED1 155 - 160 cm	1.124	<0.100	<0.100	-	1.50	-	-	-
YUK15-YED1 198 - 202 cm	1.319	<0.100	<0.100	-	-	-	-	-
YUK15-YED1 295 - 301 cm	2.363	0.155	1.410	9.075	16.91	-	-	-24.64
YUK15-YED1 409 - 417 cm	2.254	0.130	1.318	10.129	13.71	-206.29	-28.81	-24.40
YUK15-YED1 450 - 457 cm	2.166	0.124	1.293	10.422	13.14	-206.52	-28.87	-24.40
YUK15-YED1 548 - 557 cm	2.628	0.101	1.306	12.907	11.55	-206.75	-29.43	-23.78
YUK15-YED1 586 - 593 cm	2.005	<0.100	1.056	10.560	12.23	-206.84	-29.55	-24.34
YUK15-YED1 655 - 662 cm	1.651	0.101	1.107	10.924	12.75	-208.25	-29.65	-24.97
YUK15-YED1 685 - 691 cm	2.237	<0.100	<0.100	-	0.54	-207.65	-28.94	-
YUK15-YED1 1005 - 1010 cm	1.835	<0.100	<0.100	-	0.61	-	-	-
YUK15-YED1 1069 - 1074 cm	0.841	<0.100	<0.100	-	1.12	-221.59	-30.70	-
YUK15-YED1 1163 - 1167 cm	0.456	<0.100	<0.100	-	1.40	-219.98	-30.32	-
YUK15-YED1 1206 - 1212 cm	0.633	<0.100	<0.100	-	1.36	-218.59	-29.75	-
YUK15-YED1 1256 - 1259 cm	0.684	<0.100	<0.100	-	1.28	-216.14	-29.24	-
YUK15-YED1 1315 - 1322 cm	0.386	<0.100	<0.100	-	1.47	-212.54	-28.74	-
YUK15-YED1 1364 - 1374 cm	0.413	<0.100	<0.100	-	1.37	-209.59	-28.27	-
YUK15-YED1 1414 - 1419 cm	0.805	<0.100	<0.100	-	1.26	-206.17	-27.96	-
YUK15-YED1 1467 - 1472 cm	0.357	<0.100	<0.100	-	-	-	-	-
YUK15-YED1 1560 - 1566 cm	0.442	<0.100	<0.100	-	-	-199.90	-27.69	-
YUK15-YED1 1632 - 1640 cm	0.882	<0.100	<0.100	-	1.52	-	-	-
YUK15-YED1 1677 - 1681 cm	0.755	<0.100	<0.100	-	-	-	-	-
YUK15-YED1 1711 - 1717 cm	0.578	<0.100	<0.100	-	-	-201.39	-27.55	-
YUK15-YED1 1758 - 1762 cm	0.538	<0.100	<0.100	-	-	-	-	-
YUK15-YED1 1820 - 1828 cm	0.842	<0.100	<0.100	-	1.28	-201.13	-27.22	-
YUK15-YED1 1853 - 1858 cm	0.302	<0.100	<0.100	-	-	-	-	-
YUK15-YED1 1920 - 1927 cm - A (sand)	0.375	<0.100	<0.100	-	1.45	-197.42	-26.52	-
YUK15-YED1 1920 - 1927 cm - B	1.927	<0.100	0.881	8.811	8.80	-198.02	-26.64	-24.91
YUK15-YED1 1996 - 2001 cm	1.873	0.110	1.012	9.202	6.16	-187.20	-25.70	-24.66
YUK15-YED1 2033 - 2039 cm	2.458	0.160	1.703	10.644	17.50	-184.63	-25.44	-25.00
YUK15-YED1 2076 - 2081 cm	2.407	0.143	1.528	10.673	11.41	-183.76	-25.31	-25.57
YUK15-YED1 2135 - 2145 cm	1.918	0.152	1.390	9.151	16.11	-182.44	-25.30	-25.27
YUK15-YED1 2207 - 2212 cm	0.836	<0.100	<0.100	-	1.01	-181.25	-25.16	-

Table 3 - Alas1 - sedimentary data

Sample	depth [cm BS]	absolut ice content [wt%]	magnetic susceptibility (low frequency) [10^{-8} m^3 kg^{-1}]	clay [vol%]	silt [vol%]	sand [vol%]	bulk density [g/cm^3]
YUK15-Alas1 7 - 11 cm	9	23.06	50.772	7.3	76.4	16.3	1.42
YUK15-Alas1 58 - 64 cm	61	22.12	90.617	5.3	71.0	23.7	1.45
YUK15-Alas1 101 - 105 cm	103	18.27	106.823	6.9	77.7	15.4	-
YUK15-Alas1 152 - 155 cm	153.5	22.97	99.246	8.8	75.0	16.1	1.42
YUK15-Alas1 197 - 201 cm	199	18.84	126.696	8.9	77.8	13.3	-
YUK15-Alas1 340 - 349 cm	344.5	19.08	126.692	7.9	77.8	14.3	-
YUK15-Alas1 390 - 400 cm	395	12.94	129.232	6.8	47.4	45.8	-
YUK15-Alas1 453 - 460 cm	456.5	12.54	156.328	6.5	30.3	63.2	-
YUK15-Alas1 645 - 650 cm	647.5	15.20	213.130	1.5	17.0	81.4	-
YUK15-Alas1 808 - 817 cm	812.5	14.74	272.920	0.7	3.4	96.0	-
YUK15-Alas1 834 - 840 cm	837	18.96	177.118	3.0	33.2	63.8	-
YUK15-Alas1 914 - 925 cm	919.5	16.72	302.377	2.1	23.4	74.5	-
YUK15-Alas1 950 - 960 cm	955	25.56	122.629	4.7	79.2	16.1	1.33
YUK15-Alas1 1088 - 1095 cm	1091.5	19.90	112.297	7.5	74.0	18.5	-
YUK15-Alas1 1147 - 1161 cm	1154	23.28	65.358	8.3	79.1	12.5	1.41
YUK15-Alas1 1201 - 1210 cm	1205.5	21.86	72.102	8.7	81.1	10.2	1.46
YUK15-Alas1 1218 - 1222 cm	1220	25.42	72.532	8.2	79.2	12.6	1.33
YUK15-Alas1 1271 - 1277 cm	1274	24.44	81.226	10.1	78.4	11.6	1.37
YUK15-Alas1 1307 - 1317 cm	1312	23.76	92.490	9.3	78.0	12.7	1.39
YUK15-Alas1 1391 - 1410 cm	1400.5	15.32	268.690	4.0	35.8	60.2	-
YUK15-Alas1 1460 - 1468 cm	1464	16.74	266.667	1.3	12.1	86.6	-
YUK15-Alas1 1527 - 1534 cm	1530.5	20.60	118.259	5.7	69.7	24.6	1.51
YUK15-Alas1 1587 - 1593 cm	1590	20.96	98.682	5.5	70.5	24.0	1.50
YUK15-Alas1 1690 - 1701 cm	1695.5	21.81	90.058	4.9	73.0	22.0	1.46
YUK15-Alas1 1754 - 1764 cm	1759	22.91	133.930	6.2	76.7	17.1	1.42
YUK15-Alas1 1790 - 1798 cm	1794	20.64	87.283	6.0	70.7	23.3	1.51
YUK15-Alas1 1897 - 1903 cm	1900	20.52	73.187	5.2	68.7	26.1	1.51
YUK15-Alas1 1963 - 1972 cm	1967.5	20.50	62.146	7.6	78.7	13.7	1.52

Table 4 - Alas1 - chemical data

Sample	TC [wt%]	TN [wt%]	TOC [wt%]	TOC/CN ratio	TOC [kg/m³]	δ2D [‰ vs. SMOW]	δ18O [‰ vs. SMOW]	δ13C [‰VPDB]
YUK15-Alas1 7 - 11 cm	3.336	0.198	2.372	11.951	33.60	-	-	-27.24
YUK15-Alas1 58 - 64 cm	1.294	<0.100	<0.100	-	1.45	-130.37	-13.44	-
YUK15-Alas1 101 - 105 cm	1.235	<0.100	<0.100	-	-	-131.30	-13.33	-
YUK15-Alas1 152 - 155 cm	1.637	0.110	<0.100	0.913	1.42	-	-	-
YUK15-Alas1 197 - 201 cm	1.092	<0.100	<0.100	-	-	-	-	-
YUK15-Alas1 340 - 349 cm	1.185	<0.100	<0.100	-	-	-	-	-
YUK15-Alas1 390 - 400 cm	0.775	<0.100	<0.100	-	-	-	-	-
YUK15-Alas1 453 - 460 cm	0.628	<0.100	<0.100	-	-	-	-	-
YUK15-Alas1 645 - 650 cm	0.460	<0.100	<0.100	-	-	-	-	-
YUK15-Alas1 808 - 817 cm	0.239	<0.100	<0.100	-	-	-	-	-
YUK15-Alas1 834 - 840 cm	0.806	<0.100	<0.100	-	-	-	-	-
YUK15-Alas1 914 - 925 cm	0.622	<0.100	<0.100	-	-	-	-	-
YUK15-Alas1 950 - 960 cm	2.467	<0.100	<0.100	-	1.33	-135.85	-15.28	-
YUK15-Alas1 1088 - 1095 cm	1.956	<0.100	<0.100	-	-	-	-	-
YUK15-Alas1 1147 - 1161 cm	1.929	<0.100	<0.100	-	1.41	-136.02	-15.48	-
YUK15-Alas1 1201 - 1210 cm	1.655	<0.100	<0.100	-	1.46	-	-	-
YUK15-Alas1 1218 - 1222 cm	1.619	0.117	0.836	7.165	11.14	-	-	-24.06
YUK15-Alas1 1271 - 1277 cm	1.714	0.186	1.069	5.746	14.61	-	-	-24.82
YUK15-Alas1 1307 - 1317 cm	2.084	0.172	1.120	6.497	15.60	-	-	-24.18
YUK15-Alas1 1391 - 1410 cm	0.520	<0.100	<0.100	-	-	-	-	-
YUK15-Alas1 1460 - 1468 cm	0.404	<0.100	<0.100	-	-	-137.58	-15.44	-
YUK15-Alas1 1527 - 1534 cm	1.201	0.111	0.823	7.447	12.44	-	-	-24.67
YUK15-Alas1 1587 - 1593 cm	1.220	<0.100	0.816	8.155	12.21	-	-	-24.30
YUK15-Alas1 1690 - 1701 cm	1.359	<0.100	0.888	8.885	13.01	-	-	-24.91
YUK15-Alas1 1754 - 1764 cm	2.307	0.199	1.769	8.877	25.16	-	-	-25.67
YUK15-Alas1 1790 - 1798 cm	1.284	<0.100	0.787	7.867	11.88	-	-	-24.28
YUK15-Alas1 1897 - 1903 cm	1.290	<0.100	0.840	8.401	12.73	-	-	-24.42
YUK15-Alas1 1963 - 1972 cm	1.383	0.101	0.866	8.594	13.13	-	-	-24.71

Table 5 - radiocarbon dating

Sample	^{14}C age [yr BP]	σ [yr BP]	material	Modelled ages [mod yr BP]	Calibrated ages [cal yr BP]	Mean age [cal yr BP]
YUK15-YED1 155-160 cm	18 064	± 104	bulk organic material	21 922 - 28 263	21 582 - 22 221	21 890
YUK15-YED1 295-301 cm	25 973	± 88	bulk organic material	28 295 - 32 071	29 822 - 30 640	30 268
YUK15-YED1 586-593 cm	35 965	± 184	bulk organic material	35 225 - 39 272	40 116 - 41 118	40 608
YUK15-YED1 1632-1640 cm	49 000	± 0	bulk organic material	45 979 - 80 155	infinite age	> 49 000
YUK15-YED1 1996-2001 cm	45 854	± 501	bulk organic material	46 031 - 101 739	48 202 - calib. limit	49 232
YUK15-Alas1 197-201 cm	12 826	± 57	bulk organic material	14 963 – 15 672	15 144 – 15 548	15 287
YUK15-Alas1 808-817 cm	23 615	± 151	bulk organic material	28 189 – 29 828	27 478 - 27 976	27 729
YUK15-Alas1 1527-1534 cm	42 647	± 364	bulk organic material	34 163 - 62 415	45 172 - 46 619	45 870
YUK15-Alas1 1963-1972 cm	39 027	± 251	bulk organic material	34 106 - 89 734	42 478 - 43 262	42 865

Acknowledgements

I carried out my master thesis at the Alfred Wegener Institute Helmholtz Centre for Polar and Marine Research in Potsdam in the Permafrost Research Section in 2018, so I would like to thank first of all the whole section and most of all the PETA-CARB group who were very supportive in any type of struggling.

The biggest thanks go to my supervisors Jens Strauss and Guido Grosse for supporting me in any possible way and always having an open ear for discussing unexpected findings and all minor problems along the way. Some very special thanks for my dear colleague, lab partner, lab supporter and friend Dyke Scheidemann who ran the labs in such a perfect way to enable a smooth lab routine for frustration-free results.

Another big thanks go out to my AWI colleagues Lutz Schirrmeister, Sebastian Wetterich, Michael Angelopoulos and Loeka Jongejans as well as to Mathias Ulrich from Leipzig University and Christine Siegert, who always came up with new interpretations in every direction and who provided the necessary scientific experience and field experience.

I also want to thank all my friends for listening to all these scientific findings over and over, to my family for supporting and enabling full concentration on this thesis and to my fiancée for supporting me through all the different and sometimes difficult phases of this writing process.

Independence statement / Eigenständigkeitserklärung

Eidesstattliche Erklärung zur Masterarbeit

Ich versichere, diese Arbeit selbständig und lediglich unter Benutzung der angegebenen Quellen und Hilfsmittel verfasst zu haben.

Alle Stellen, die wörtlich oder sinngemäß aus veröffentlichten oder noch nicht veröffentlichten Quellen entnommen sind, sind als solche kenntlich gemacht.

Die Zeichnungen oder Abbildungen in dieser Arbeit sind von mir selbst erstellt worden oder mit einem entsprechenden Quellennachweis versehen.

Ich erkläre weiterhin, dass die vorliegende Arbeit noch nicht im Rahmen eines anderen Prüfungsverfahrens eingereicht wurde.

Potsdam, den _____ _____

Statutory Declaration

I declare that I have authored this thesis independently, that I have not used other than the declared sources / resources

and that I have explicitly marked all material which has been quoted either literally or by content from the used sources.

Furthermore I declare that this thesis has not been submitted for any other exam.

Potsdam, _____ _____